Non-essential kinetochore proteins contribute to meiotic chromosome condensation through polo-like kinase

Authors: Deepika Trakroo[#], Prakhar Agarwal[#], Anushka Alekar, and Santanu Kumar Ghosh*

Affiliation: Department of Biosciences and Bioengineering, Indian Institute of Technology, Bombay, Powai, Mumbai-400076, India.

# Equal contribution

*Corresponding author

Email: santanughosh@iitb.ac.in

Tel. +(91-22) 2576 7766

Key words: Meiosis, chromosome, kinetochore, condensin, budding yeast

Abstract

Chromosome condensation plays a pivotal role during faithful chromosome segregation, hence understanding the factors that drive condensation is crucial to get mechanistic insight into chromosome segregation. Previously we showed that in budding yeast, the absence of the non-essential kinetochore proteins affects chromatin-condensin association in meiosis but not in mitosis. A differential organization of the kinetochores, that we and others observed earlier during mitosis and meiosis may contribute to the meiotic-specific role. Here, with our in-depth investigation using in vivo chromosome condensation assays in cells sans a non-essential kinetochore protein, Ctf19, we establish that these proteins have roles in achieving a higher meiotic condensation without influencing much of the mitotic condensation. We further observed an accumulation of the polo-like kinase Cdc5 owing to its higher protein stability in *ctf19Δ* meiotic cells. High Cdc5 activity causes hyper-phosphorylation of the condensin resulting in its reduced stability and concomitant decreased association with the chromatin. Overall, our findings highlight the role of Ctf19 in promoting meiotic chromosome condensation by influencing the activity of Cdc5 and thereby affecting the stability and association of condensin with the chromatin.

Introduction

Faithful chromosome segregation across eukaryotes requires that the chromosomes become condensed and attached properly to the microtubule spindle during cell division. The attachment is mediated by a conserved multiprotein complex called 'kinetochore' formed at the centromeres of the chromosomes (Cleveland et al., 2003, Ishi and Akiyoshi., 2022). The proteins within a kinetochore are organized in a hierarchical fashion with respect to the centromeric DNA and the microtubules (Biggins., 2013, Cheeseman and Desai., 2008, De Wulf et al., 2003, Westermann et

43 al., 2007). The inner and the outer proteins associate with the centromeres and microtubules,
44 respectively whereas the central proteins act as linker (Meraldi et al., 2006, Dong et al., 2022, Dou
45 et al., 2023). Over the last three decades studies on kinetochore from myriad organisms have
46 revealed that this protein complex, besides establishing a connection with the microtubules, also
47 controls other cellular activities that facilitate high-fidelity chromosome segregation (Glynn et al.,
48 2004, Muller et al., 2012, Meyer et al., 2015, Kim et al., 2013). In budding and fission yeasts, the
49 kinetochore proteins, in particular the essential inner and central proteins, are also shown to
50 promote chromosome condensation (Kruitwagen et al., 2018, Nakazawa et al., 2008).

51 Chromosome condensation is promoted by an evolutionarily conserved condensin
52 complex, which binds to the chromatin facilitating its condensation through DNA compaction,
53 formation of DNA loops, and its axial shortening (Freeman et al., 2000, Strunnikov et al., 1995,
54 Kruitwagen et al., 2015). Condensation in budding yeast is established in prophase and persists till
55 the end of mitotic division (Vas et al., 2007, Lamothe et al., 2020). The cell cycle-dependent
56 chromatin-condensin association is regulated by several factors. While CDKs initiate this during
57 start of the cell cycle, Polo-like kinase and Aurora B kinase maintain it during metaphase, possibly
58 through phosphorylation of their substrates, including the condensin complex (Giet et al., 2001,
59 Lavoie et al., 2004, St. Pierre et al., 2009). Such timely association and resulting accurate folding
60 of the chromatin are critical for faithful chromosome segregation.

61 The kinetochore complex also plays a crucial role in chromatin-condensin association..
62 Several studies have revealed that this role is executed through kinetochore-mediated centromeric
63 and pericentromeric recruitment of several proteins including cohesins (Guacci et al., 1997, Lavoie
64 et al., 2004), shugoshin (Peplowska et al., 2014, Kruitwagen et al., 2018, Yahya et al., 2020), 14-
65 3-3 protein, Bmh1 (Jain et al., 2021) and enzymes such as aurora B kinase, Ipl1 (Giet et al., 2001,
66 Petersen et al., 2003, Lavoie et al., 2004,), polo-like kinase, Cdc5 (St. Pierre et al., 2009, Bazile

67 et al., 2010, Leonard et al., 2015, Lamothe et al., 2020) and a histone deacetylase, Hst2 (Wilkins
68 et al., 2014, Kruitwagen et al., 2015, 2018, Jain et al., 2021). However, the non-essential proteins
69 of the Ctf19 sub-complex (Ctf19c) of the kinetochore (Mehta et al., 2022) were not shown to
70 hinder chromosome condensation (Kruitwagen et al., 2018) as expected from their dispensability
71 in mitotic growth. However, we have shown earlier that in absence of these non-essential proteins,
72 meiosis is severely affected as several meiosis specific events are perturbed (Ghosh et al., 2004,
73 Mehta et al., 2014, Agarwal et al., 2015). This happens as there appears to be a differential
74 organization of the kinetochore assembly between mitosis and meiosis (Mehta et al., 2014, Borek
75 et al., 2021) for which the non-essential proteins perhaps facilitate certain protein-protein and/or
76 protein-DNA interactions in meiosis but not in mitosis.

77 Strikingly, earlier we observed that Ctf19 has a role to play in meiotic chromosome
78 condensation since the cells in the absence of Ctf19 harbor defects in rDNA condensation and
79 show reduced association of condensin with the chromatin in meiosis but not in mitosis (Mehta et
80 al., 2014). While why chromatin-condensin association is compromised in *ctf19Δ* meiotic cells is
81 not known, we hypothesize that to facilitate prophase I events, meiosis may require extra
82 chromosome condensation than mitosis, and the nonessential kinetochore proteins might
83 contribute to regulating that. This notion is also fueled by the distinct thread-like appearance of
84 the paired homologous chromosomes in pachytene of meiosis I, which is never visible in mitosis
85 and unlikely to happen in meiosis solely due to pairing.

86 In this report, to test the above hypothesis we sought to compare the extent of chromosome
87 condensation between mitosis and meiosis and to find a molecular explanation of condensation
88 defect in the non-essential kinetochore mutants. Interestingly, we observed using three cell
89 biological in vivo assays that the chromosomes indeed appeared more condensed in meiosis than
90 in mitosis. We further demonstrate that lack of Ctf19 causes misregulation of Cdc5 specifically in

91 meiosis, which leads to hyper-phosphorylation of condensin resulting its dissociation from the
92 chromatin and defect in chromosome condensation. Additionally, using wild type cells
93 overexpressing Cdc5, we show that the misregulation of Cdc5 is indeed the reason for condensin
94 failing to associate properly with the chromatin. This study highlights yet another meiosis-specific
95 essential contribution of the mitotically dispensable kinetochore proteins.

96 **Results**

97 **Chromosomes are more condensed in meiosis as compared to mitosis**

98 We hypothesize that the level and determinants of chromosome condensation might differ between
99 mitosis and meiosis because earlier, using Ctf19c mutant, we observed that the kinetochore has a
100 role in rDNA condensation in meiosis but not in mitosis (Mehta et al., 2014). However, whether
101 such a role is confined to a specific condensed locus like rDNA or it is observed at other
102 chromosomal locales remains unknown. To investigate this, we first sought out to compare the
103 extent of chromosomal condensation of the kinetochore proximal pericentromeric regions between
104 mitosis and meiosis. Diploid strains were constructed where one copy of chromosome V was
105 marked with $[TetO]_{224}$ –[TetR-GFP] system at a locus 1.4 kb away from the *CEN V* (henceforth
106 called *CEN V*-GFP). The fluorescence intensity of *CEN V*-GFP was used as a surrogate marker to
107 decipher the in vivo condensation level, as described before (Kruitwagen et al., 2015). In this
108 microscopy-based assay, the fluorescence intensity of TetR-GFP bound to the $[TetO]_n$ array
109 inserted at a decondensed locus will be more compared to when the array is inserted at a condensed
110 locus. This is because, due to condensation, a linear shrinkage of the operators happens, which
111 brings the TetR-GFP molecules closer to each other, causing quenching of the fluorescence and,
112 hence, reduction in the intensity (Fig. 1A). The *CEN V*-GFP marked strains also harbored SPBs
113 (Spc42) marked with mCherry to judge different cell cycle stages. The GFP signal intensities were

114 measured in the cells residing at the pre-S phase (interphase) stage or at metaphase/metaphase I,
115 which is presumed to contain decondensed and condensed chromatin, respectively. An unbudded
116 cell with a single SPB was taken as a pre-S phase cell in mitosis or meiosis; a large budded cell
117 with two separated SPBs in the mother compartment was taken as a metaphase cell (Fig. 1B)
118 whereas same in an unbudded meiotic cell was considered as a metaphase I cell (Fig. 1C). The
119 timepoint to harvest meiotic pre-S phase cells was determined based on Ime1 (an inducer of
120 meiosis in yeast) expression and FACS analysis. The Ime1 expression is induced by an acetate-
121 based rich medium (YPA), however, it starts accumulating in the nucleus after the depletion of G1
122 cyclins (Colomina et al., 1999, 2003). In our experimental condition also, Ime1 expression started
123 in YPA, followed by its nuclear localization around 30 mins in SPM with no nuclear localization
124 either in YPA or hardly any in SPM at 10 mins (Fig. S1A, B). FACS analysis showed that the
125 DNA synthesis started before the cells were at least 90 mins in SPM (Fig. S1C), which is consistent
126 with the earlier studies reporting that the initiation of premeiotic S phase in SK1 yeast strain
127 happens around 60 mins in SPM (Borner et al., 2023, Cha et al., 2000). Hence, 1 hr in SPM was
128 taken as the timepoint to harvest meiotic pre-S phase cells for our assays. For metaphase I cells,
129 the sample was harvested at 6 hrs in SPM, and cells with SPB-SPB distance more than 1 but less
130 than 3 μm were analyzed as described before (Tsuchiya et al., 2014, Yu and Koshland, 2005). The
131 mitotic pre-S phase was determined based on Cln2 expression (yeast G1/S-CDK) as its expression
132 marks the beginning of mitosis (Hadwiger et al., 1989) (Fig. S1D).

133 The *CEN V*-GFP signal intensity normalized with the background intensity was measured
134 from four different types of samples – mitotic interphase, metaphase, meiotic interphase, and
135 metaphase I cells as described in materials and methods. As expected, both in mitosis and meiosis,
136 the *CEN V*-GFP fluorescence intensity decreases in the metaphase and metaphase I cells,
137 respectively, than in the corresponding interphase cells reconfirming that condensation occurs as

138 the cells proceed into the M phase of the cell cycle. (Lavoie et al., 2004; Vas et al., 2007).
139 Interestingly, while in mitosis, the extent of decrease was 31.2% (2389 vs. 1643 A.U., Fig. 1B),
140 the same was 39.6% (2136 vs. 1289 A.U., Fig. 1C) in meiosis. Notably, the signal intensity was
141 observed ~1.3-fold lesser in meiotic metaphase samples as compared to mitotic metaphase I (1289
142 vs. 1643 A.U.). Such a decrease in signal intensity in meiosis over mitosis argues for an increased
143 level of chromosome condensation in meiosis than in mitosis. Since *CEN V*-GFP fluorescence
144 intensity was measured from different mitotic and meiotic cells, an error in measuring the intensity
145 across the samples may lead to the observed difference in fluorescence intensity between mitosis
146 and meiosis. To rule out this possibility we mixed the mitotic and meiotic cells and measured the
147 fluorescence intensity from the metaphase or metaphase I cells residing in the same field of view.
148 The metaphase cells with two SPBs and a bud were distinguishable from the metaphase I cells
149 harboring 2 SPBs but no bud. Consistent with the previous observation, we found ~1.5-fold
150 decreases in signal intensity in meiotic metaphase I cells compared to mitotic metaphase cells
151 (3252 vs. 2198 A.U., Fig. 1D), indicating chromosomes are indeed more condensed in meiosis
152 than in mitosis.

153 **The non-essential kinetochore protein Ctf19 influences chromosome condensation in**
154 **meiosis but not in mitosis**

155 Earlier we and others have reported that the mitotically non-essential kinetochore proteins have
156 essential roles in meiosis (Mehta et al., 2014, Agarwal et al., 2015, Borek et al., 2021). In support
157 of this, we observed that such a protein, Ctf19, promotes rDNA condensation in meiosis but not
158 in mitosis (Mehta et al., 2014). Since we revealed that the extent of chromosome condensation, at
159 least at the pericentromeres, is more in meiosis than in mitosis, we wished to investigate the
160 contribution of Ctf19 to this difference. We measured the *CEN V*-GFP signal intensity in the
161 diploid *ctf19Δ* mutant cells from the pre-S phase and metaphase/metaphase I in both mitosis and

162 meiosis. Any meiosis-specific function of Ctf19 on condensation is expected to ameliorate the
163 difference in condensation (or *CEN V*-GFP signal intensity) between the pre-S phase and M phase
164 in meiosis but not in mitosis. We observed a significant (44.2%) decrease in signal intensity in
165 metaphase cells compared to the pre-S phase cells in the *ctf19Δ* mutant (3195 vs 1789 A.U., Fig.
166 2A) similar to the wild type (Fig. 1B) suggesting that condensation is not compromised in the
167 mutant compared to the wild type in mitosis. In contrast, in meiosis, unlike the wild type, which
168 showed a 39.6% decrease in the intensity in meiosis (Fig. 1C), only around 6.5% decrease (4182
169 vs 3913 A.U., Fig. 2B) was found in the mutant, which was not statistically significant indicating
170 that a meiosis-specific chromosome condensation defect occurs in absence of Ctf19. Notably,
171 although the interphase intensity was observed higher in *ctf19*Δ than in the wild type irrespective
172 of the type of the cell cycle, the mutant achieves a level of chromatin condensation similar to the
173 wild type during mitotic metaphase, but not during meiotic metaphase I (Fig 2C). This suggests
174 that while the *ctf19*Δ mutation might also have subtle condensation defect in mitosis, its impact is
175 more substantial during meiosis.

176 To examine if the observed condensation defect in the *ctf19*Δ mutant in meiosis is specific
177 to the Ctf19c proteins of the kinetochore, we monitored the *CEN V*-GFP signal in the pre-S phase
178 and metaphase I stage in the cells lacking Slk19, another non-essential protein residing at the
179 kinetochore but not as a component of the Ctf19c (Zeng et al., 1999). We could not observe any
180 chromosome condensation defect in the *slk19*Δ cells as the GFP signal intensity decreased in
181 metaphase I compared to the interphase stage (~45%, 592 vs 321 A.U., Fig. S2A). Since we used
182 identical conditions during mitosis and meiosis, the possibility of other factors viz., accessibility
183 of TetR-GFP to the operators or a lower concentration of TetR-GFP responsible for reducing the
184 fluorescence intensity, can be void. Moreover, the control mutant *slk19Δ* behaved as expected.

185 To further establish that the observed condensation defect in the *ctf19*Δ is not due to an
186 artifact of the assay employed above, we used an alternative in-vivo assay to further validate the
187 observed condensation defect. We evaluated the condensation status in meiosis and mitosis for
188 both the wild type and *ctf19*Δ by using Second Harmonic Generation (SHG) microscopy which
189 relies on generating a second harmonic by the chromatin fibers upon excitation by two-photon
190 microscopy (Yamin et al., 2020, 2022). In this assay, the chromosomes were stained with DAPI
191 and a higher ratio of integrated density to area obtained through the SHG technique corresponds
192 to higher condensation. As expected, we indeed observed an increased condensation in both wild
193 type and *ctf19*Δ in mitotic metaphase as compared to pre-S phase (Fig. 3 A, B). However, when
194 the meiotic cells of the same strains were analyzed, the wild type cells showed significant increase
195 in the ratio of integrated density to area at metaphase I as compared to pre-S phase, but the *ctf19*Δ
196 cells did not show any significant increase in the ratio in meiotic metaphase I (Fig. 3 C, D). These
197 findings further confirm that the *ctf19*Δ cells are indeed compromised in meiotic condensation
198 with no significant effect on mitotic condensation.

199 Since in budding yeast the rDNA condensation can be monitored in a better way than the
200 rest of the chromosomes, for further validation of the condensation defect in the *ctf19* mutant, we
201 compared the extent of rDNA condensation using Net1-GFP as the marker as described before
202 (Torres-Rosell et al., 2004, Machín et al, 2005, Mehta et al., 2014) among the wild type, *ctf19*Δ,
203 and *slk19*Δ strains (Fig. S2B). The Net1-GFP signal pattern was visualized in these strains when
204 the cells were arrested at the metaphase I stage (*pCLB2-CDC20*). While around 85% of the wild-
205 type cells showed the 'tight knit' and 'crescent' signal which represent a condensed state of rDNA
206 (Mehta et al., 2014; Kerr et al., 2011), *ctf19*Δ cells showed a reduction (50%) in the frequency and
207 a corresponding increase (50%) in the occurrence of the 'puff' signal which corroborates a
208 decondensed state. On the other hand, *slk19*Δ cells showed similar results to the wild type. In

209 mitosis, however, there was no difference in condensation amongst the wild type, *ctf19*Δ, and
210 *slk19*Δ cells (Fig. S2C) where the 'line', 'loop', and 'puff' patterns designate condensed,
211 intermediate, and decondensed forms of the rDNA locus, respectively (D'Ambrosio et al., 2008;
212 Dauban et al., 2019). Altogether, from these results, we infer that Ctf19 promotes chromosome
213 condensation in meiosis but not in mitosis, and this function appears to be specific for the Ctf19
214 protein or perhaps for all the non-essential proteins of the Ctf19c of the kinetochore.

215 **Loss of Ctf19 affects axial condensation of the chromosomal arm**

216 The loss of pericentric and rDNA condensation in the *ctf19*Δ mutant prompted us to examine the
217 mutant for linear (axial) condensation of the chromosomal arms which relies on condensin
218 (Kruitwagen et al., 2015). To investigate this, we marked chromosomes at two different loci 400
219 kb away from each other, one was near the *CEN V* (1.4 kb away), as before, and the other one was
220 21 kb away from *TEL V* using $[TetO]_{224}$ –[TetR-GFP] and $[TetO]_{448}$–[TetR-GFP] systems,
221 respectively. Since the number of operators used to visualize *TEL V*-GFP was double that of *CEN*
222 *V*-GFP, the two loci could be visually distinguishable by the brightness of the GFP dots where
223 *TEL V*-GFP appeared much brighter than the *CEN V*-GFP (Fig. 4A, B). In the wild type, we
224 observed a 37% decrease in the mean distance in the metaphase I stage (0.568 µm) compared to
225 the pre-S phase stage (0.83 µm) owing to the condensation (Fig. 4C, left panel). However, in the
226 *ctf19Δ* mutant, there was no significant decrease in the mean distances between the two stages
227 (1.00 vs. 1.167 µm), suggesting a defect in the condensation (Fig. 4C, right panel). While looking
228 at the axial condensation in mitosis, there was a statistically significant decrease in the distance in
229 metaphase compared to the pre-S phase both in the wild type and the mutant (21% and 24 %,
230 respectively) (Fig. S3 A, B). Notably, since the mean distance in the mutant (1.16 µm) was found
231 higher than the wild type (0.83 µm) in the meiotic pre-S phase that precedes condensin function,
232 it is possible that at this phase, the compaction of the chromatin is compromised in the mutant due

233 to relaxed nucleosome-nucleosome interaction or probably due to subtle defects acquired during
234 preceding mitotic cycle. Altogether, these results suggest that the contribution of Ctf19 in
235 promoting chromatin condensation in meiosis is not only restricted to the pericentromeric regions
236 but also extends axially along the chromosome arms at the distal loci.

237 **Ctf19 is required for maintenance of chromatin-condensin association in meiosis.**

238 Earlier, we reported that in the absence of Ctf19, the chromatin-condensin association is perturbed
239 in meiosis (Mehta et al., 2014), which supports our findings from the condensation assays
240 described here. We wished to re-verify our earlier observation with further investigation to find
241 whether the effect on chromatin-condensin association is specific to Ctf19c proteins and whether
242 the effect is on the establishment and/or maintenance of the association. To address these, we first
243 compared the localization of the condensin protein Brn1 on the chromatin between the wild type
244 and *ctf19Δ* mutant along with the *slk19Δ* mutant, which, as a control, showed no effect on
245 condensation (Fig. S2A and S2B). Brn1 fused to 6XHA at the C-terminal (Verzijlbergen et al.,
246 2014) was detected on the chromatin in the meiotic cells arrested at metaphase I by Cdc20
247 depletion. While a similar number (~ 13 to 15) of bright Brn1-6HA foci were visible in the wild
248 type and *slk19Δ* mutant, the number of foci was much lower (~7), and the foci were less bright in
249 the *ctf19Δ* mutant suggesting a defect in chromatin-condensin association in the latter (Fig. S4 A).
250 On the other hand, as expected from the condensation assay results, no difference in Brn1-6HA
251 localization was observed between the wild type and *ctf19*Δ spreads prepared from the cells
252 arrested at mitotic metaphase by Cdc20 destruction as mentioned in materials and methods (Fig.
253 S4 B, C). To test if the observed condensation defect is specific to Ctf19 or also occurs in other
254 non-essential proteins of Ctf19c, we analyzed the association of Brn1-6HA with chromatin in cells
255 lacking another protein of Ctf19c, Ctf3. We found that in *ctf3Δ* cells also, the number of Brn1-
256 6HA foci was lesser (~4) than the wild type (~9) (Fig. S5). The lesser number of foci here in the

257 wild type compared to the previous chromatin spread of Brn1-6HA in the wild type (Fig. S4) can
258 be because of technical difference in antibody staining, as these experiments were performed at
259 different times

260 To further validate our chromatin spread data from meiosis, we performed a ChIP assay to
261 quantify the association of Brn1 with different regions of chromosome – centromere,
262 pericentromere, and arm (Fig. 5A). The cells were harvested after 8 and 10 hrs into SPM to obtain
263 metaphase I arrested wild type and *ctf19Δ* mutant, respectively by Cdc20 depletion. The time
264 points were chosen based on our previous observations where the *ctf19*Δ cells showed a delay in
265 the meiotic cell cycle and were arrested maximally at metaphase I at 10 hrs into SPM (Mehta et
266 al., 2014). We observed a significant reduction in the level of Brn1 at all the regions in the mutant
267 compared to the wild type; however, the reduction was more at the centromeric region compared
268 to other regions (Fig. 5B). These results, re-confirming our earlier chromatin spread data (Mehta
269 et al., 2014), further indicate that the meiotic defect in chromatin-condensin association is specific
270 to the lack of Ctf19c proteins.

271 Next, we wished to address whether Ctf19 is required for the establishment or maintenance
272 of chromatin-condensin association. It has been previously shown that during early meiosis,
273 condensin first associates with rDNA as a cluster and then at later time points associates with the
274 rest of the chromatin, leaving a minuscule amount at the rDNA (Markowitz et al., 2020; Li et al.,
275 2014). To compare the dynamics of chromatin-condensin association between wild type and
276 *ctf19Δ* we monitored the association of Brn1-6HA with chromatin using chromatin spreads at
277 different time points in the cells released into synchronized meiosis (Fig. 5C). Types 1 – 2 are
278 categorized as localization of Brn1-6HA first at rDNA (type 1) and then gradually spreading to
279 rest of the chromatin (type 2). Type 3 implies a gross reduction in chromatin-condensin
280 association. While the initial rDNA localization of Brn1-6HA (0 hr, type 1) in the mutant was not

281 found lesser than the wild type, its gross chromatin localization (type 2) in the mutant was merely
282 below 10% of the spreads compared to the wild type (40%) at 4 hrs. The spreads with type 2
283 localization of Brn1 did not increase in the mutant even at the later time points (~10% at 8 hrs),
284 while the spreads from wild type cells showed about ~50% type 2 localization at the same time
285 points. This implies that the establishment of condensin association with the gross chromatin, but
286 not with the rDNA, is perturbed in the absence of Ctf19. Consequently, at 8 hrs, while the mutant
287 showed a major population of spreads (70%) with reduced condensin on the chromatin (type 3),
288 only a minor population (<10%) of wild type spreads demonstrated this phenotype. The phenotype
289 of reduced chromatin association of Brn1 (type 3) in the mutant starts to appear as early as 4 hrs
290 and keeps on increasing as the cells undergo the meiotic cell cycle (Fig. 5C). Moreover, the type
291 1 population also decreased to <10% in the mutant, while about 50% of the wild type cells retained
292 the type 1 population at 8 hrs; these observations may be interpreted as a defect in the maintenance
293 of the rDNA association of condensin in the mutant.

294 **The condensation defect in *ctf19*Δ may occur partially through Sgo1 mislocalization but**
295 **independent of DDK- and Ipl1-mediated pathways**

296 Next, we wished to address the mechanism through which Ctf19 may regulate condensation in
297 meiosis. Besides protecting the pericentromeric cohesin in meiosis I, Sgo1 (Shugoshin) has a role
298 in mitotic chromosome condensation (Kruitwagen et al., 2018) through condensin loading at
299 pericentromeric region (Peplowska et al., 2014). It has also been reported that in the absence of
300 Ctf19c proteins, Iml3 and Chl4, the Sgo1 localization becomes compromised at the chromatin both
301 in mitosis (Deng et al., 2018) and meiosis (Kiburz et al., 2005). To investigate if Ctf19, unlike the
302 peripheral Ctf19c components Iml3 and Chl4, differs in recruiting Sgo1 on the chromatin between
303 mitosis and meiosis which may cause the differential effect on condensation, we analyzed the
304 localization of Sgo1-EGFP in mitosis (metaphase) and meiosis (metaphase I) in presence or

305 absence of Ctf19. We observed that the absence of Ctf19 affected Sgo1 localization both in mitosis
306 (Fig. 6A) and meiosis (Fig. 6B), however, the extent of the defect was more in meiosis where 81%
307 of the cells showed Sgo1-EGFP mislocalization (no signal) compared to only 57% in mitosis.
308 Whereas the fraction of cells showing no signal of Sgo1-EGP in the wild type was found similar
309 in mitosis and meiosis (Fig. 6A, B). To further validate our cell biological data, we performed a
310 ChIP assay to quantify the association of Sgo1-9Myc with the centromeres. We observed a
311 significant reduction in the level of Sgo1-9Myc at the centromeres both in mitosis (Fig. 6C) and
312 meiosis (Fig. 6D) in *ctf19*Δ mutant compared to the wild type, while the reduction was non-
313 significant at a negative locus, *TUB2.* However, the reduction was more (~86% (0.2114 vs 0.03)
314 for *CEN III* and ~82% (0.2497 vs 0.043) for *CEN IV*) in meiosis than in mitosis (~ 45% (0.4290
315 vs 0.2376) for *CEN III* and ~ 40% (0.3745 vs 0.2254) for *CEN IV*) (Fig. 6C, D; see materials and
316 methods). Based on these observations, we conclude that a higher reduction in Sgo1's association
317 with the chromatin in meiosis over mitosis in *ctf19*Δ cells may contribute partially, if at all, to the
318 meiosis-specific chromatin-condensin association defect in these cells.

319 It has been reported earlier that till metaphase the rDNA condensation in mitosis is
320 dependent on cohesin (Lavoie *et al*., 2002). As the cohesin loading at the pericentromeres is
321 dependent on Ctf19 through recruitment of DDK (Dbf4-dependent kinase) both in mitosis and
322 meiosis (Hinshaw et al., 2015, 2017), therefore, the reduction of cohesin level at the centromeres
323 in *ctf19*Δ mutant is unlikely the cause for observed meiosis-specific condensation defect. However,
324 recently DDK and Cdc5 (budding yeast polo-like kinase) have been reported to have roles in the
325 meiotic prophase-like pathway (cleavage-independent cohesin removal from the chromatin) which
326 has been shown important for chromosome compaction in meiosis probably by making space on
327 chromatin for condensin loading (Challa et al., 2019). Based on this, we hypothesized that perhaps
328 DDK kinase localization at the centromeres is perturbed in the absence of Ctf19, which in turn

329 results in an impaired prophase-like pathway, hence leading to chromosome condensation defect.
330 If our hypothesis is correct, then a DDK mutant unable to be localized at the centromeres should
331 show a condensation defect in meiosis. It has been reported that the fusion of epitopes at the C-
332 terminal of the Dbf4 protein renders it inactive at the centromeres however, its localization at the
333 origins of replications remains unaffected (Hinshaw et al., 2017). We constructed a strain
334 expressing Dbf4-9myc with heterozygous tagging of *CEN V* and *TEL V* with GFP. We confirmed
335 that the *DBF4-9MYC* allele is acting as a mutant, as we observed a reduced frequency of sister
336 chromatid cohesion (Fig. S6A) as reported earlier (Hinshaw et al., 2015). However, we failed to
337 observe any defect either in axial contraction by measuring the distance between *CEN V* and *TEL*
338 *V* (Fig. S6B) or in condensation of centromeric and telomeric regions measured by fluorescence-
339 based quenching assay (Fig. S6C). Here, in meiosis, although we observed that the distances
340 between the two loci are more than the wild type (Fig 4B), but the extent of axial compaction from
341 pre-S phase to metaphase I was found similar in both the conditions viz., ~1.4 fold in the wild type
342 (0.8308 vs 0.5686 μm) while ~1.2 fold in the DDK mutant (1.179 vs 0.9591 μm). Based on these
343 observations we conclude that the absence of DDK at the centromeres in *ctf19Δ* cells is not
344 responsible for the observed condensation defect in these cells in meiosis.

345 Phosphorylation of histone H3 at serine 10 by Aurora kinase B (Ipl1 in budding yeast) has
346 been known to play a crucial role in chromosome compaction both in yeast (Kruitwagen et al.,
347 2015) and mammals (Mora-Bermúdez et al., 2007). Additionally, an in vitro assay has
348 demonstrated an interaction between Ctf19 and Ipl1, which is essential for stabilizing the
349 chromosomal passenger complex (CPC) at the centromeres (Fischböck-Halwachs et al., 2019).
350 However, it is uncertain whether Ctf19 interacts with Ipl1 in vivo and regulates Ipl1's centromeric
351 localization and possibly thereby promotes chromosome condensation in meiosis. To address this
352 question, we performed a ChIP assay to quantify the association of Ipl1 at the centromeres in

353 metaphase I arrested wild-type and *ctf19*Δ mutant cells, harvested at 8 and 10 hours into SPM,
354 respectively. However, our analysis did not reveal any significant reduction in the centromeric
355 enrichment of Ipl1 in the *ctf19Δ* mutant compared to the wild type (Fig. S7). Based on these
356 findings, we conclude that Ctf19 does not regulate Ipl1 localization at the centromeres, at least
357 during meiosis, and hence Ctf19's involvement in chromosome condensation is independent of the
358 Ipl1-mediated pathway.

359 **Polo-like kinase (Cdc5) level increases in the cells in the absence of Ctf19 in meiosis**

360 Having shown that DDK and Ipl1 kinases are not involved, we wished to identify other factor(s)
361 that may promote meiotic condensation via Ctf19. A kinase switch model for chromosome
362 condensation says that different kinases take turns to regulate the condensation at different stages
363 of the cell cycle (Bazile et al., 2010). For instance, casein kinase II, cyclin-dependent kinase, and
364 polo-like kinase regulate condensation at the interphase, metaphase, and anaphase, respectively.
365 Recently, in budding yeast, the polo-like kinase Cdc5 has been shown to be important for both
366 condensation establishment and maintenance in mitosis (Lamothe et al., 2020). Furthermore,
367 earlier, we reported that in meiosis, Ctf19c protein mutants show SPB misduplication and
368 supernumerary SPBs (Agarwal et al., 2015), a phenotype also noticed in meiotic cells
369 overexpressing Cdc5 (Shirk et al., 2011). Therefore, we wished to examine if there is any meiosis-
370 specific misregulation of Cdc5 in the *ctf19*Δ cells, which might cause the condensation defect.
371 Surprisingly, we observed a higher level of Cdc5 in the *ctf19*Δ cells in meiosis but not in mitosis
372 when the cells were arrested at metaphase I and metaphase, respectively (Fig. 7A and Fig. S8A).
373 To investigate if the high level is due to increased stability of Cdc5 and/or high expression of the
374 corresponding gene, we first detected the protein level of Cdc5-6HA over time in meiosis after
375 blocking the protein synthesis using cycloheximide (CHX) which was added at 8 hrs and 10 hrs
376 timepoints when the wild type and mutant cells were into SPM medium, respectively. We found

377 that Cdc5 is more stable in the mutant compared to the wild type (Fig. 7B). The difference between
378 the slopes of the lines was significant as calculated using GraphPad Prism 8.0.1 ($p = 0.009$).
379 However, we failed to observe any increased stability of Cdc5 in the mutant in mitosis (Fig. S8B).
380 To examine if the higher level of Cdc5 in the mutant is due to transcriptional alteration of *CDC5*
381 gene, we measured its transcript level in the wild type and *ctf19*Δ cells used in Fig. 7A. We did
382 not observe any increased expression of the *CDC5* gene in the mutant (Fig. S8C). From these
383 results, we conclude that perhaps increased stability and a consequent higher level of Cdc5 in
384 *ctf19*Δ cells in meiosis cause the condensation defect.

385 Despite the high level of Cdc5, its association with chromatin was reduced in *ctf19*Δ mutant
386 compared to the wild type as observed by chromatin spread in meiosis (Fig. 7C). We observed a
387 significant increase in the population of spreads with reduced Cdc5 signal (type II) in the *ctf19*Δ
388 strain compared to the wild type during meiosis. However, this difference was not significant
389 during mitosis (Fig. 7D). The reduction in Cdc5-chromatin association can be possible because of
390 reduced cohesin association with chromatin in the absence of Ctf19 (Mehta et al., 2014, Hinshaw
391 et al., 2017). In the absence of cohesin, the chromatin localization of Cdc5 is compromised and its
392 activity becomes somehow misregulated causing hyper-phosphorylation of condensin subunits
393 leading to condensation defect (Lamothe et al., 2020). Therefore, we hypothesized that the
394 increased level of chromatin unbound Cdc5 in *ctf19*Δ meiotic cells may misregulate the condensin
395 phosphorylation status resulting in a reduced association of condensin with the chromatin with
396 consequent condensation defect (Fig. 5). To test this hypothesis, we monitored the phosphorylation
397 status of the condensin protein Ycg1, as it is an essential subunit for condensin complex
398 recruitment to chromatin (Piazza et al., 2014) and is known to be phosphorylated at multiple sites
399 (St-Pierre et al., 2009). We monitored Ycg1-6HA expression pattern over different time points in
400 cells released synchronously into meiosis till metaphase I arrest (Fig. 8A). At later time points (8

401 hrs and 10 hrs) in SPM, which corresponded to the metaphase I arrested stage, two bands of higher
402 (B1) and lower (B2) mobilities were visible while at early time points (0 and 6 hrs) only one band
403 was visible both in wild type and mutant indicating post-translational modification of Ycg1-6HA
404 as reported earlier (St-Pierre et al., 2009). Since the B1 bands at 6 hrs are of higher intensity
405 compared to the bands at 0 hr, we speculated that 0 and 6 hrs bands harbor unmodified and
406 (unmodified + modified) forms of Ycg1-6HA, respectively. However, it was interesting to note
407 that in the mutant the top band B2 was reproducibly of higher intensity compared to the wild type.
408 We speculated that the B2 band depicts a higher-level modification of Ycg1-6HA and was found
409 more in the mutant compared to the wild type. Treatment of the protein extract from metaphase I
410 arrested cells with lambda phosphatase showed that the modification is phosphorylation (Fig. 8B).
411 A better resolution of the protein bands using Phos-tag gel revealed that B1 band indeed contained
412 unphosphorylated and phosphorylated forms of Ycg1-6HA whereas B2 band harbored hyper-
413 phosphorylated Ycg1-6HA (Fig. 8B). These results suggest that hyper-phosphorylation of
414 condensin protein in the mutant possibly occurs due to excess Cdc5 level in the mutant as observed
415 earlier.

416 It is possible that the hyper-phosphorylated form of Ycg1 in the mutant is less stable which
417 impedes the chromatin-condensin association in the mutant. Similar effect on the chromatin-
418 condensin association was observed for Brn1 subunit of the condensin complex (Fig. 5). To verify
419 this, we monitored the Ycg1 level in the CHX chase experiment where the protein synthesis was
420 blocked by adding the drug at 8 hrs and 10 hrs in SPM for the wild type and the mutant,
421 respectively; the samples were harvested at the indicated time points (Fig. 8C). We found that
422 Ycg1 is indeed less stable in the mutant compared to the wild type. The difference between the
423 slopes of the lines depicting the Ycg1 level was also significant, as calculated using GraphPad
424 Prism 8.0.1 ($p = 0.03$). We also tested whether the Ycg1 stability was also impaired in the *ctf19*Δ

425 cells in mitosis. For that, we first arrested both the wild type and *ctf19*Δ cells in metaphase by
426 nocodazole (Fig. S9A) and then added CHX in the media to monitor Ycg1 stability. We found no
427 difference in the Ycg1 stability in the wild type and *ctf19*Δ cells (Fig. S9B, C), indicating that
428 Ctf19 influences the stability specifically in meiosis. From our results, we conclude that higher
429 stability of Cdc5 causes accumulation of the protein in *ctf19*Δ meiotic cells, which results in hyper-
430 phosphorylation of condensin. This hyper-phosphorylated condensin is less stable and possibly
431 why its association with the chromatin decreases (Fig. 5, S10).

432 **Misregulation of Cdc5 influences chromatin-condensin association**

433 If excess Cdc5 is responsible for reduced chromatin-condensin association in *ctf19*Δ meiotic cells,
434 then overexpression of Cdc5 in the wild type cells should emulate that, whereas its depletion
435 should rescue the defect in the mutant. The overexpression of Cdc5 in the wild type was achieved
436 by shuffling the endogenous promoter of *CDC5* with the *CUP1* promoter. Since overexpression
437 of Cdc5 leads to multiple Spc42 foci (Song et al., 2000), we used this phenotype to optimize the
438 concentration of copper to be used for normal and overexpression of Cdc5. While the cells grown
439 in 20 μM $CuSO_4$ in YPD showed very few cells with >2 Spc42-EGFP foci, the same was increased
440 significantly when the cells were grown in 50 μM or higher concentration of $CuSO_4$ (Figure S11).
441 Based on this, we assumed that a concentration lesser than 20 μM and higher than 50 μM of $CuSO_4$
442 can be considered as a normal and overexpression of Cdc5, respectively. We further verified the
443 overexpression in meiosis as a phenotype of metaphase I delay, as reported earlier (Shirk et al.,
444 2011, Li et al., 2014). We see a gradual drop in the percentage of cells with metaphase I spindle
445 from 7 hr to 9 hr (59% to 42%) when the cells were treated with 10 μM $CuSO_4$ in SPM. However,
446 the cells grown in 50 μm $CuSO_4$ did not show the drop (49% to 46%) suggesting sustained
447 metaphase I delay due to over expression of Cdc5 (Fig S12A, B). The cells were released into
448 SPM either in 10 or in 50 μm $CuSO_4$ and were harvested at 7 hr (Fig. 9A), since this time point

449 produced a maximum number of metaphase I cells while treated with 50 μm $CuSO_4$ (Fig. S12B).
450 In the harvested cells, when we visualized the level of chromatin-condensin association using
451 chromatin spreads, the normal level of Cdc5 (10 μm $CuSO_4$) produced 11 to 13 bright Brn1-6HA
452 foci, while with excess Cdc5 (50 μm $CuSO_4$), the number was much lower (~7) (Fig. 9B, C, S12
453 C) indicating a defect in the association which is consistent to an earlier report (Li et al., 2014).

454 Next, to examine if the defect in chromatin-condensin association in the *ctf19*Δ meiotic
455 cells can be rescued by depleting Cdc5, we shuffled the *CDC5* promoter with *CUP1* promoter in
456 those cells and followed the above strategy except used 0 μm $CuSO_4$ instead of 50 μm (Fig. 9D).
457 We verified that at 7-8 hrs of SPM release, maximum number of metaphase I cells were present
458 (Fig. S12D, E). With normal level of Cdc5 (10 μm $CuSO_4$), we observed around 6 Brn1-6HA foci,
459 while with no Cdc5 expression (0 μm $CuSO_4$), we could see a significantly higher number of Brn1-
460 6HA foci (~10) (Fig. 9E, F, S12 F) indicating a clear amelioration of the defect. Taken together,
461 the above results suggest that the observed meiosis specific condensation defect in the absence of
462 Ctf19 is indeed due to accumulation of Cdc5 in the cells.

463 **Discussion**

464 For the last few decades, the kinetochore-centromere has emerged as a controlling hub for various
465 events of chromosome segregation viz., kinetochore-microtubule attachment, early replication of
466 centromeres, pericentromeric cohesin enrichment, homolog pairing, and chromosome
467 condensation. In budding yeast, the essential kinetochore proteins have been shown to initiate
468 chromosome condensation in *cis* which is believed to extend distal to the centromeres through
469 Sgo1 and a histone deacetylase, Hst2 (Kruitwagen et al., 2018). On the other hand, through a series
470 of studies, we and others have demonstrated that the organizational assembly of the kinetochore
471 complex differs between mitosis and meiosis and possibly due to this difference it was found that

472 the mitotically non-essential kinetochore proteins play significant roles in meiosis; consequently,
473 in their absence, meiosis is very poor but not mitosis (Mehta et al., 2014, Agarwal et al., 2015,
474 Borek et al., 2021). In this work, we demonstrate that the mitotically dispensable kinetochore
475 proteins contribute to achieve a higher chromatin condensation in meiosis through regulating the
476 activity of Cdc5 polo-like kinase.
477
478 **Chromosome condensation: mitosis vs meiosis**
479 Regardless of the mode of the cell cycle, chromosomes need to be condensed as they embark into
480 partitioning. However, there are fundamental differences in how the chromosomes behave as they
481 enter into mitosis or meiosis (meiosis I, in particular). One of the major differences is the pairing
482 of the homolog in meiosis which is believed to start at the centromeres by 'centromere coupling'
483 (Tsubouchi et al., 2005) and proceeds towards the telomeres in a zipper-like fashion. It is obvious
484 that finding the right partners and the completion of lengthwise pairing will be more efficient if
485 the units undergoing pairing are shorter and more condensed. Moreover, the post-pairing events,
486 including chiasmata formation and resolution of the chiasmata by 'terminalization' of the cross-
487 over point, are also presumably favored by more condensed chromosomes. Notably, in pachytene
488 during meiosis I, the paired homologs are individually visible as thread-like structures by whole
489 chromatin staining using DAPI even in small yeast nuclear spreads. However, although the
490 homologs never pair in mitosis, they never appear as thread-like structures even with half the DAPI
491 intensity of the pachytene spreads. By using two different methods of in vivo condensation assays,
492 we observed that in budding yeast meiotic chromosomes are indeed more condensed than the
493 equivalent mitotic stage chromosomes (Fig. 1, 4C, S3A-B). However, since we observed a greater
494 decrease in intensity of GFP foci and distance between them, as readout for chromatin's local
495 compaction and global contraction, respectively, in meiosis, both nucleosome-nucleosome

496 interaction and condensin function may culminate into higher meiosis-specific condensation.
497 Evidence of more chromosome condensation in meiosis is available in nature. For instance, in Rye
498 (*Secale cereale*) it is reported that chromosomes are compacted in meiosis by a factor of 1.7 in
499 length and 1.3 in diameter more compared to mitosis (Zoller et al., 2004). Notably, we found ~1.5
500 times more condensation in meiosis compared to mitosis by in vivo assay in budding yeast (Fig.
501 1D) indicating a similar mechanism across eukaryotes might exist to achieve more chromosome
502 condensation in meiosis.
503

504 **Kinetochore proteins controlling chromosome condensation**

505 Chromosome condensation can be divided into two stages viz., establishment and maintenance,
506 which are regulated by kinases. As the cells enter into the cell cycle, the condensin becomes active
507 and condensation is established through CDKs (Kimura et al., 1998, Sutani et al., 1999). After the
508 metaphase to anaphase transition, as the CDK level starts declining, aurora B kinase and polo-like
509 kinases phosphorylate condensin subunits and thus maintain the condensation (Lavoie et al., 2004,
510 Takemoto et al., 2007, St. Pierre et al., 2009, Walters et al., 2014, Kruitwagen et al., 2018). In
511 budding yeast mitosis, the essential inner kinetochore proteins promote condensation at the
512 centromeres/pericentromeres by recruiting Ipl1 (aurora B) and Cdc5 (polo-like) kinases at the
513 centromeres (Lavoie et al., 2004, St. Pierre et al., 2009). In contrast, the outer essential and the
514 inner non-essential kinetochore proteins were found to be dispensable for condensation (Nakazawa
515 et al., 2008, Kruitwagen et al., 2018) possibly because they do not regulate chromatin localization
516 of Ipl1 and Cdc5. However, given our earlier study reporting meiosis specific reduction in
517 chromatin-condensin association in absence of the non-essential kinetochore protein Ctf19 (Mehta
518 et al., 2014), in this study we show that the effect is specific to the lack of Ctf19c proteins and it
519 is the establishment of the association which is compromised.

520 Since our and other studies showed reduced pericentric cohesin enrichment in *ctf19*Δ cells
521 (Mehta et al., 2014, Fernius and Marston 2009), it can be argued that the observed reduction in
522 chromatin-condensin association in *ctf19*Δ meiotic cells is merely due to pericentric cohesin
523 enrichment defect. This can happen provided i) compared to mitosis, in meiosis, the arm cohesin
524 is sufficiently low due to the meiosis-specific prophase-like pathway of cohesin removal (Challa
525 et al., 2019), which becomes aggravated due to simultaneous loss of cohesin from the
526 preicentromeres and ii) the presence of cohesin must promote condensin binding. But we
527 categorically negate the above possibilities because i) half of the arm cohesin still remains after
528 cohesin removal by a prophase-like pathway (Challa et al., 2019) although earlier works failed to
529 detect any significant difference in arm cohesin between mitosis and meiosis (Glynn et al., 2004,
530 Fernius and Marston 2009) and ii) it was shown that cohesin does not influence condensin binding
531 using biochemical and cell biological assays (Lamothe et al., 2020, Lavoie et al., 2002).
532 Condensation distal from the centromeres can be influenced by non-essential kinetochore
533 proteins through Bub1 and DDK kinases mediated recruitment of Sgo1 (Fernius et al., 2007,
534 Peplowska et al., 2014) and cohesin (Lavoie et al., 2004, Natsume et al., 2013, Hinshaw et al.,
535 2015), respectively, at the pericentromeres which is then believed to extend towards the telomeres
536 through functions of Sgo1 and Hst2 (Kruitwagen et al., 2018). Therefore, we tested whether Sgo1's
537 centromeric localization and DDK activity are further down in meiosis in *ctf19*Δ cells to explain
538 meiosis-specific condensation defects in these cells. We failed to see any effect on condensation
539 in DDK-compromised cells (Fig. S6A, B and C). However, a higher reduction of Sgo1 level at the
540 pericentromeres in meiosis than in mitosis in *ctf19Δ* cells (Fig. 6) argued this as a possible cause
541 of meiosis-specific condensation defect in these cells. Additionally, we observed that the
542 centromeric association of Ipl1 kinase remains unaffected in *ctf19Δ* cells, indicating that Ctf19
543 does not play a regulatory role in condensation through the Ipl1-mediated pathway (Fig. S7).

544 Further studies surprisingly revealed that it is the higher accumulation of Cdc5 in the *ctf19*Δ
545 meiotic cells that perturbs chromatin-condensin association as discussed below.
546
547 **Interaction of kinetochore with polo-like kinase**
548 In budding yeast, the polo-like kinase Cdc5 is targeted to the centromeres through interaction with
549 the kinetochore proteins in mitosis (Snead et al., 2007, Mishra et al., 2019). It is also shown that
550 pericentromeric cohesin enriches Cdc5 at the centromeres which in turn promotes cohesin removal
551 (Mishra et al., 2016). Therefore, as *ctf19Δ* cells show reduced pericentric cohesin enrichment
552 (Fernius et al., 2009, Mehta et al., 2014), it is expected that the association of Cdc5 with the
553 chromatin would be less, and that is what we observed (Fig. 7C). But more reduction of Cdc5-
554 chromatin association in meiosis than in mitosis (Fig. 7D) may account for a greater effect of
555 pericentric cohesin loss in meiosis in *ctf19*Δ cells. Earlier, it was reported that the Cdc5 dislodged
556 from the chromatin due to global cohesin inactivation, hyper-phosphorylates condensin which
557 remains bound to the chromatin and is stimulated to misfold the chromatin into a decondensed
558 state (Lamothe et al., 2020). We also noticed hyper-phosphorylation of condensin (Fig. 8A, B),
559 but in contrast observed a huge drop in chromatin-condensin-association in the spreads made from
560 *ctf19Δ* cells (Fig. 5, S4A, S10), possibly because the hyper-phosphorylated condensin generated
561 in our conditions is less stable (Fig. 8C). Notably, while Lamothe et al., 2020, could not find the
562 difference in total Cdc5 level between wild type and cohesin-depleted cells, we observed a
563 substantial increase in Cdc5 level in *ctf19Δ* cells compared to the wild type. That might have
564 caused a different type of hyper-phosphorylation of condensin in our cells compared to their
565 conditions, leading to the dissociation of condensin from the chromatin. Therefore, we conclude
566 that in *ctf19Δ* cells, the meiosis-specific altered behavior of Cdc5 is not only due to pericentric
567 cohesin reduction but also due to its higher stability (Fig. 7B). Currently, it is not known that how

568 the loss of Ctf19 leads to a higher stability of Cdc5 in meiosis. Cdc5 has meiosis-specific roles
569 including degradation of Pds1 in meiosis I (Attner et al., 2013), mono-orientation of sister
570 chromatids by regulating the association of Mam1 protein with kinetochores, step-wise cohesin
571 removal (Lee and Amon, 2003) and dissolution of homolog linkage (Yu and Koshland, 2005).
572 Moreover, unlike mitosis, in meiosis, Cdc5 is degraded by APC associated with meiosis-specific
573 co-factor Ama1 (Okaz et al., 2012). Therefore, a meiosis-specific protein-protein interaction
574 involving Cdc5 is expected. In this context, given a difference in the assembly of kinetochore
575 exists between mitosis and meiosis (Mehta et al., 2014, Borek et al., 2021), the loss of Ctf19 and
576 possibly other non-essential proteins of Ctf19c might create a condition that disfavors normal
577 degradation of Cdc5. One possibility is that in the *ctf19*Δ mutant cells the activity of Mnd2, an
578 antagonist to Ama1 (Oelschlaegel et al., 2005), increases as Mnd2 is believed to physically interact
579 with Ctf19 (Wong et al., 2007). It will be interesting to investigate the status of Mnd2 and Ama1
580 in the *ctf19*Δ mutant.

581 Overall, in this work, we reveal that the chromosomes are more condensed during meiosis
582 than in mitosis which has implications for understanding the complex meiotic chromosome
583 behavior in mammals where the gametogenesis is largely asymmetric and mechanistically varies
584 profoundly between the sexes. In animal cells, there is no evidence of kinetochore inactivation
585 affecting chromosome condensation in meiosis. Since we observed that the non-essential proteins
586 affect condensation in meiosis but not in mitosis, it would be intriguing to examine the
587 condensation status in animal meiotic cells harboring mutations in kinetochore. Finally, the
588 interaction between kinetochore integrity and the functionality of polo-like kinase (Plk) can be
589 explored in animal cells as improper polo-like kinase activity has been linked to aneuploidy and
590 different disease states in humans viz., elevated Plk level has been reported in several types of
591 cancers and neurological disorders (Takai et al., 2005, Ackermann et al., 2011, Korns et al., 2022).

592 **Material and methods**

593 **Yeast strains**

594 All the strains utilized in this work were derived from the SK1 background and are mentioned in
595 Table S1. Chromosome V was fluorescently marked near *CEN V* and *TEL V* using $[TetO]_n$ –[TetR-
596 GFP] system in strains expressing TetR-GFP. An array of 224 copies of the TetO sequence was
597 inserted at locus 1.4 kb away from *CEN V* through homologous recombination (Michaelis et al.,
598 1997, Tanaka et al., 2000). Similarly, $[TetO]_{448}$ array was inserted near *TEL V* between *BMH1* and
599 *PDA1* genes (Kumar et al., 2021). To perform gene deletion, promoter shuffling, and C-terminal
600 tagging of proteins, a PCR-based method was used (Wach, 1996, Longtine et al.,1998, Janke et
601 al., 2004). Relevant plasmid-borne cassettes procured from Euroscarf were employed for these
602 techniques. Yeast transformation was performed as described previously (Guldener et al., 1996).

603 The cells were synchronized in the G1 phase in the YPA medium and then released in YPD
604 and SPM for mitotic and meiotic sample collection, respectively. For the mitotic pre-S phase, the
605 cells were harvested at 45 mins post-release in YPD which corresponds with the start of Cln2
606 expression. The cells were identified microscopically by unbudded cells with one SPB focus. For
607 metaphase, the cells were harvested after 1.5 hrs post-release in YPD and distinguished
608 microscopically by large-budded cells with two SPB foci in the mother bud. For meiosis, the cells
609 were harvested at 1 hr and 6 hrs post-release in SPM for pre-S phase and metaphase I cell,
610 respectively.

611

612 **Meiotic synchronization**

613 Meiotic induction was carried out as described elsewhere (Cha et al., 2000). Typically, the diploid
614 strain of interest was streaked onto a YPD plate (1% yeast extract, 2% peptone, 2% dextrose, 2%
615 agar) for a single colony followed by 48 hrs of incubation. A single colony was then inoculated
616 into 5 ml of YPD broth and left to incubate overnight at 30°C for ~15 hrs. Subsequently, cells from
617 the overnight grown culture were transferred to a 50 ml YPA medium (1% yeast extract, 2%
618 peptone, and 1% potassium acetate) at 0.2 OD_{600} and grown till ~1.4-1.6 OD_{600} which took
619 approximately 13-15 hrs. 1 ml of YPA culture was taken, the cells were diluted appropriately and
620 subjected to sonication at 50% amplitude for 3 secs and observed under microscope for G1 arrest.
621 Once over 85% of G1 arrest was achieved, the cells were washed with sterile distilled water and
622 resuspended in 50 ml of sporulation media (SPM; 0.3% potassium acetate and 0.02% raffinose).
623 Meiotic synchronization was performed at 30°C with continuous shaking at 200 RPM. Samples
624 were harvested from the SPM at specified time intervals for further experimentation. For
625 metaphase I arrest, the cells harboring *CDC20* promoter shuffled with mitotic *CLB2* promoter (Lee
626 and Amon, 2003), were harvested at 8 hrs and 10 hrs for wild type and *ctf19*Δ mutant, respectively.

627 **The arrest of yeast strains at mitotic metaphase**

628 *Using the auxin-induced degron system*

629 Mitotic metaphase arrest was achieved by degrading Cdc20 using the AID degron (Auxin-
630 Inducible Degron) system (Nishimura et al., 2009). In cells expressing *OsTIR1* from the *ADH1*
631 promoter, the AID coding sequence was C-terminally fused to *CDC20*. Cells were grown in YPD
632 from 0.2 to 0.5 OD_{600} before auxin (3-Indoleacetic acid, Sigma) was added at 1.5 mM
633 concentration and the culture was incubated for a further 2 hrs at 30ºC. Metaphase arrest was
634 confirmed by DAPI staining (more than 85% large budded cells with undivided DAPI).

635 *Using nocodazole, a microtubule depolymerizing drug*

636 The cells were inoculated in YPD at 0.2 OD_{600} and grown till 0.5-0.6 OD_{600} before nocodazole (20
637 µg/ml, Sigma) was added to the culture which was incubated for a further 2 hrs under shaking
638 conditions at 30ºC. Metaphase arrest was confirmed by DAPI staining.

639 **Fluorescence microscopy**

640 The cells were grown in YPD or SPM medium for mitotic or meiotic culture, respectively. The
641 cells were harvested and fixed with 4% formaldehyde for 5 mins and then washed twice with 0.1
642 M phosphate buffer before imaging. All fluorescence images were acquired with a Zeiss Axio
643 Observer.Z1 (63X objective, NA = 1.40; Carl Zeiss Micro-Imaging Inc.) equipped with Axiocam
644 camera. The images were processed and analyzed using Zeiss Zen 3.1 software. Image J and Imaris
645 (8.0.2) software were used for intensity and distance measurements, respectively. For all the box
646 plots for the intensity and distance measurements, mean values were compared across the samples.

647 **Intensity measurement**

648 For intensity calculation of a fluorescence signal, Z-stacks with maximum intensity were merged.
649 A Region Of Interest (ROI) was drawn around the signal of interest, and the integrated density was
650 determined to get the 'signal intensity'. ROI of the same size was put elsewhere in the nucleus for
651 background signal and integrated density was determined to get the 'background intensity'. Each
652 signal intensity value was normalized with the background intensity values to get the 'normalized
653 signal intensity' which was used to plot the graphs. For *CEN V*-GFP intensity comparison between
654 pre-S phase cells and metaphase I cells in meiosis, the normalized signal intensity obtained from
655 metaphase I cells was divided by 2 to obtain intensity per *CEN V*-GFP as at this stage two sister
656 centromeres are glued together by cohesin and two sister *CEN V*-GFP dots appeared as a single
657 dot (Fig S13).

658 **Second Harmonic Generation (SHG) microscopy and analysis**

659 The sample preparation for SHG microscopy was followed as mentioned earlier (Yamin et al.,
660 2020; 2022). Briefly, the cells were harvested and fixed in 4% paraformaldehyde for 20 mins at
661 RT; they were washed with 0.1 M phosphate buffer and stained with DAPI (Invitrogen, #D1306)
662 for 20 mins in dark. The cells were subsequently placed on a polylysine coated slide and allowed
663 to adhere to the slide. After washing the immobilized cells with PBS, mounting solution was added
664 and the slide was covered with a coverslip. Cells were then analyzed by a Zeiss LSM780 inverted
665 Confocal Microscope, with multi-photon Chameleon vision II Laser (laser power > 3 W, pulse
666 width and repetition rate at default settings, tuning range 690‑1040 nm); Lambda−PMT−
667 identifying all the wavelength spectrums. The slides were excited by 768 nm and emission was
668 collected at 414-628 nm. The quantification was carried out using ImageJ software as mentioned
669 earlier (Yamin et al., 2020; 2022).

670 **Chromatin spread and the analysis**

671 Chromatin spread was performed by following the protocol mentioned elsewhere (Mehta et al.,
672 2014) with certain modifications. Cells were harvested from the mitotic culture of 1.0 OD_{600} and
673 at the required time point for meiotic culture. The cells were washed once with spheroplasting
674 solution (1.2 M sorbitol in 0.1 M phosphate buffer) and harvested by centrifugation at 3000 RPM
675 for 3 mins. The cells were resuspended in 0.5 ml of spheroplasting solution supplemented with 5
676 µl of β-mercaptoethanol and 12.5 µl of zymolyase 20T (10 mg/ml, MP Biomedicals) and incubated
677 at 30ºC for 1.5 hrs. Once 80-90% of the cells were spheroplasted (by observing under the
678 microscope), the spheroplasting was stopped by adding 1 ml of ice-cold stop solution (0.1 M MES
679 - pH 6.4, 1 mM EDTA, 0.5 mM $MgCl_2$, 1 M Sorbitol). The spheroplasts were centrifuged at 2000
680 RPM for 3 mins at 4 ºC and resuspended gently in 125 µl of ice-cold stop solution. 60 µl of

681 spheroplasted cells were put on acid-washed glass slides followed by the addition of 40 µl of
682 fixative solution (4% paraformaldehyde, 3.4% sucrose, 10 N NaOH) and 80 µl of 1% lipsol (LIP
683 Equipment and services) over it. After gentle mixing 80 µl of fixative solution was again added to
684 the slides. The content on the slides was mixed and spread gently using a pipette tip and kept at
685 room temperature overnight for drying. The slides were then washed with 2 ml of 0.4% photo
686 flow-200 (Kodak) and then submerged in 1X PBS for 15 mins. The excess liquid was removed
687 and 100 µl of blocking solution (10 mg/ml BSA in 1X PBS + 5% Skim milk) was immediately
688 added over the fixed nuclear spreads which were then covered with coverslips and incubated at
689 room temperature in a humid chamber for 20 mins. The coverslips were removed and 100 µl of
690 primary antibody (1:200) was added to each slide and incubated at room temperature for 60 mins.
691 The primary antibody was rinsed off by submerging the slides 3 times in 1X PBS for 5 mins each
692 and 100 µl of secondary antibody (1:200) was added followed by incubating at room temperature
693 for 60 mins. The slides were again washed in the same way followed by incubation with 100 µl of
694 DAPI (1 µg/ml, Invitrogen) for 30 mins. After PBS wash for 5 mins, 100 µl of mounting solution
695 (90% glycerol supplemented with 1 mg/ml p-phenylenediamine) was added over the slides
696 followed by a clean coverslip which was sealed with transparent nail paint. The primary antibodies
697 used: rat anti-HA (3F10, Roche), mouse anti-HA (12CA5, Roche) and rat anti-Tubulin (MCA78G,
698 Serotec). The secondary antibodies used: Rhodamine (TRITC)-conjugated goat anti-Rat (Jackson)
699 and Alexa Fluor 488 conjugated goat anti-Mouse IgG (Jackson).

700 For calculation of the number of fluorescence foci associated with each chromatin spread,
701 all the Z-stacks with the signals were first merged and then the file was exported to Imaris (8.0.2)
702 software. The images were visualized using '3-D view' tool of the software. Subsequently, the
703 'Spot' tool in the algorithm setting of the software was used to mark the different foci present in

704 the chromatin spreads. The background fluorescence was subtracted using an automated
705 'subtraction' tool, and the number of foci visible for each spread was scored.

706

707 **Indirect immunofluorescence**

708 Immunofluorescence was performed, as mentioned previously (Mittal et al., 2020; Shah et al.,
709 2023). Briefly, cells from meiotic culture were harvested at indicated time points and fixed with
710 4% formaldehyde at room temperature (RT) for 15 mins. The fixed cells were washed once with
711 PBS and spheroplasted in spheroplasting solution (1.2 M sorbitol, 0.1 M phosphate buffer pH 7.5),
712 in the presence of Zymolyase 20T (MP Biomedicals, #32092) (10 mg/ml) and 25 mM β-
713 mercaptoethanol or 1 hr at 30°C. The spheroplasts were mounted on a polylysine coated slide. The
714 cells were then flattened by immersing the slide in -20°C methanol for 5 mins and in acetone for
715 30 s. The slides were dried for 1-2 mins before blocking using 5% skim milk solution prepared in
716 dilution buffer (10 mg/ml BSA in PBS). The cells were incubated with appropriate primary and
717 secondary antibodies for 1 hr at RT. Following several washes with PBS, samples were incubated
718 with DAPI (Invitrogen, #D1306) (1 µg/ml) solution for 20 mins in dark. Finally, the glass slides
719 were sealed with coverslips for imaging after spreading the mounting solution (1 mg/ml
720 phenylenediamine in 90% glycerol). The antibodies and their dilutions (in dilution buffer) were
721 mentioned as follows. Primary antibodies rat anti-tubulin (Serotec, MCA78G) at 1:5000.
722 Secondary antibodies: (TRITC)-labeled goat anti-rat (Jackson, #115485166).

723 **ChIP (Chromatin immunoprecipitation)**

724 Chromatin immunoprecipitation was performed as described previously (Makrantoni et al., 2019)
725 with certain modifications. Chromatin was cross-linked with 1% formaldehyde (30 mins for Brn1-
726 6HA, 1 hr for Sgo1-9Myc, 2 hrs for Ipl1-6HA) at 25°C with shaking of the culture at 100 RPM,

727 followed by the addition of glycine at a final concentration of 125 mM to quench the crosslinking.
728 Cells were harvested and washed twice with 10 ml ice-cold TBS buffer and once with 10 ml 1X
729 FA lysis buffer (50 mM Hepes–KOH pH 7.5, 150 mM NaCl, 1 mM EDTA, 1% Triton X-100,
730 0.1% Na-deoxycholate) supplemented with 0.1 % SDS. The cell pellet was resuspended in 500 µl
731 of ice-cold 1X FA lysis buffer supplemented with 0.5% SDS, 1 mM PMSF and 1X PIC (Protease
732 Inhibitor Cocktail, Roche). An equal volume of glass beads was added and cells were lysed in a
733 mini bead beater (BIOSPEC, India) for 9 cycles (1 min ON, 1 min OFF on ice). The lysate was
734 collected in a pre-chilled 1.5 ml eppendorf tube and centrifuged at 16,000 x g for 15 min at 4°C.
735 The supernatant was removed and the pellet was resuspended in 1 ml ice-cold 1X FA lysis buffer
736 supplemented with 0.1% SDS, 1 mM PMSF and PIC. The tubes were again centrifuged at 16,000
737 x g for 15 mins. The supernatant was discarded and the chromatin pellet was resuspended in 300
738 µl ice-cold 1X FA lysis buffer supplemented with 0.1% SDS, 1 mM PMSF and PIC. The chromatin
739 was then sheared to 300-500 bp using a water bath sonicator (Diagenode SA, Picoruptor, BC 100,
740 LAUDA Germany) for 30 cycles of 30 s ON / 30 s OFF at 4°C. The sonicated sample was then
741 centrifuged at 16,000 x g for 15 mins at 4°C. The supernatant was collected to which 1X FA lysis
742 buffer was again added and re-centrifuged at the same settings. 10 µl of the supernatant was stored
743 as input at -20°C (Whole cell extract, WCE) and the rest was divided into 'plus antibody' (+Ab)
744 and 'minus antibody' (-Ab), 600 µl each. Aliquots (+Ab) were incubated with 5 µg antibody [anti-
745 HA (3F10, Roche) or anti-MYC (AB9106, Abcam)] overnight in rotating conditions followed by
746 incubation with 50 µl of 50% Protein A Sepharose-beads (GE Healthcare,17-0780-01) for 2 hrs at
747 4°C in rotating condition. The beads were washed at room temperature twice with 1 ml of IP wash
748 buffer I (1X FA lysis buffer, 0.1%SDS, 275 mM NaCl), twice with 1 ml of IP wash buffer II (1X
749 FA lysis buffer, 0.1%SDS, 500 mM NaCl), once with 1 ml of IP wash buffer III (10 mM Tris pH
750 8.0, 250 mM LiCl, 0.5% NP-40, 0.5% sodium deoxycholate, 1 mM EDTA) and once with 1 ml of

751 1X TE (Tris EDTA). The beads were resuspended in elution buffer (50 mM Tris, pH 8.0, 10 mM
752 EDTA, 1% SDS) and incubated overnight at 65°C for de-crosslinking. De-crosslinked samples
753 were treated with Proteinase K (SRL, India) at 45 °C for 2 hrs followed by P:C:I
754 (Phenol:Chloroform:Isoamyl, Himedia) purification. Purified samples were further used for qPCR
755 analysis using CFX96 Real-Time system (BioRad) and SYBR green dye (BioRad) for detection.
756 Enrichment/Input was calculated by the following equation: $\% Encrichment/input =$
757 $E\hat{}(-\Delta \mathrm{Ct})$; where, E is the primer efficiency and was calculated by plotting Ct values of serially
758 diluted input with respect to Log dilution. E = $(-1)/\mathrm{slope}$ and $\Delta Ct = Ct_{(Test\ sample)} - (Ct_{(Input)} - Log\ E\ (Input\ dilution\ factor)$. Primers used for PCR amplification are given in Table S2. For calculation
760 of percentage decrease of Sgo1-9Myc enrichment at the centromeres in the ChIP assays (Fig 6C
761 and D) following formulae was used: $\%\ \mathrm{decrease} = \frac{WT-MT}{WT} x\ 10$; (WT and MT are average
762 enrichment/input values from the wild type and the mutant, respectively).

763

764 **Protein isolation and western blotting**

765 Samples for western blotting were prepared by resuspending the cells in 200 µl of 20% TCA.
766 Equal volume of glass beads was added, and bead beating was done using a mini bead beater
767 (BIOSPEC, India) for 5 cycles (1 min ON, 1 min OFF on ice). Supernatant was collected by
768 centrifugating at 2800 RPM for 2 mins. 400 µl of 5% TCA was again added to the beads and
769 supernatant was again collected after centrifugation. The total supernatant obtained (600 µl) was
770 centrifuged at maximum speed (13,500 RPM) for 5 mins to precipitate the protein. The supernatant
771 was removed, and the protein pellet was resuspended in Laemmli buffer and loaded on SDS-PAGE
772 after boiling at 95°C for 5 mins for further analysis. For phosphatase assay, protocol mentioned
773 elsewhere (Ontoso et al., 2013) was followed with certain modifications. TCA extract in Laemmli

774 buffer was diluted 10-fold in 1X PMP buffer (NEB, Protein Metallo Phosphatases) supplemented
775 with 1 mM $Mncl_2$. The diluted sample was treated with 2 µl Lambda protein phosphatase (NEB)
776 and incubated in water bath at 30 °C for 4 hrs. As control, a similar diluted extract but without
777 adding phosphatase was incubated at similar conditions. The protein sample was TCA precipitated
778 and resuspended in Laemmli buffer followed by heating at 95°C for 5 mins. Western blotting was
779 performed using standard procedure. The blots were developed using following antibodies: rat
780 anti-tubulin antibody (MCA78G, Serotec,), mouse anti-HA (12CA5 and 3F10, Roche), HRP-
781 conjugated goat anti-mouse IgG (Jackson), HRP-conjugated goat anti-rat (Jackson). For CHX-
782 chase experiments, the percentage of protein remaining at each time point was calculated by taking
783 the protein level at 0 hr as 100%.

784 **RNA isolation**

785 Total RNA was extracted from meiotic cell culture of 1.5-2 OD_{600} (~2.5 x10^7 cells) using TRIzol®
786 reagent and PureLink® RNA mini kit (Ambion Life Technologies™). The cell pellet was re-
787 suspended in TRIzol® and cell lysis was done using DEPC treated sterile 0.5 mm glass beads. The
788 rest of the protocol was followed as instructed by the supplier (PureLink® RNA mini kit). RNA
789 was eluted in DEPC (Sigma Aldrich Chemicals Pvt. Ltd.) treated sterile water. DNase treatment
790 was done at 37°C for 10 mins using RNAse-free DNase I (Thermo Fisher Scientific) in the buffer
791 supplied with the enzyme. The DNase and salts in the buffer were removed by purification using
792 trizol-based layer separation and pure RNA was recovered from the aqueous layer. To ensure the
793 absence of DNA impurity, end-point PCR was performed.

794 **Biological replicates and statistical methods**

795 The quantitative data shown in all the figures were obtained from two or three biological replicates.
796 The N values in the figure legends are the total number of cells analyzed from combined replicates

797 of individual assay. Box plots were generated using OriginPro software (OriginLab) and GraphPad
798 Prism 9.0 (Version 9.4.1) software. Statistical significance was estimated using two-tailed
799 student's t-test for mean with $p < .05$ considered to be significant.

800

801 **Competing Interest Statement**

802 The authors declare no competing interests

803 **Acknowledgement**

804 We acknowledge the central instrumentation facility of IIT Bombay. The SKG laboratory is
805 supported by the Science and Engineering Research Board (SERB), Govt. of India (Grant No.
806 CRG/2020/000444). DT and PA are supported by CSIR fellowships (09/087(0886)/2017- EMR-
807 I), and (09/087(0972)/2019- EMR-I), respectively. AA is supported by JRF fellowship from
808 Department of Biotechnology (DBT), Govt of India (Grant No. BT/PR43050/BRB/10/1992/2021).

809 *Author contributions*: DT, PA and AA performed experiments. DT and SKG designed
810 experiments, analyzed and interpreted the data. DT, PA and SKG wrote the manuscript.

811 **References**

812 Ackermann, S., Goeser, F., Schulte, J.H., Schramm, A., Ehemann, V., Hero, B., Eggert, A.,
813 Berthold, F. and Fischer, M., 2011. Polo-like kinase 1 is a therapeutic target in high-risk
814 neuroblastoma. *Clinical Cancer Research*, *17*(4), pp.731-741.

815 Agarwal, M., Mehta, G. and Ghosh, S.K., 2015. Role of Ctf3 and COMA subcomplexes in meiosis:
816 Implication in maintaining Cse4 at the centromere and numeric spindle poles. *Biochimica et*
817 *Biophysica Acta (BBA)-Molecular Cell Research*, *1853*(3), pp.671-684.

818 Attner, M.A., Miller, M.P., Ee, L.S., Elkin, S.K. and Amon, A., 2013. Polo kinase Cdc5 is a central
819 regulator of meiosis I. *Proceedings of the National Academy of Sciences*, *110*(35), pp.14278-
820 14283.

821 Bazile, F., St-Pierre, J. and D'Amours, D., 2010. Three-step model for condensin activation during
822 mitotic chromosome condensation. *Cell Cycle*, *9*(16), pp.3263-3275.

823 Biggins, S., 2013. The composition, functions, and regulation of the budding yeast kinetochore.
824 *Genetics*, *194*(4).

825 Borek, W.E., Vincenten, N., Duro, E., Makrantoni, V., Spanos, C., Sarangapani, K.K., de Lima
826 Alves, F., Kelly, D.A., Asbury, C.L., Rappsilber, J. and Marston, A.L., 2021. The proteomic
827 landscape of centromeric chromatin reveals an essential role for the Ctf19CCAN complex in
828 meiotic kinetochore assembly. *Current Biology*, *31*(2), pp.283-296.

829 Börner, G. V., Hochwagen, A., & MacQueen, A. J., 2023. Meiosis in budding
830 yeast. *Genetics*, *225*(2).

831 Cha, R.S., Weiner, B.M., Keeney, S., Dekker, J. and Kleckner, N., 2000. Progression of meiotic
832 DNA replication is modulated by interchromosomal interaction proteins, negatively by Spo11p
833 and positively by Rec8p. *Genes & development*, *14*(4), pp.493-503.

834 Challa, K., Shinohara, M. and Shinohara, A., 2019. Meiotic prophase-like pathway for cleavage-
835 independent removal of cohesin for chromosome morphogenesis. *Current genetics*, *65*, pp.817-
836 827.

837 Cheeseman, I. M., & Desai, A., 2008. Molecular architecture of the kinetochore-microtubule
838 interface. In *Nature Reviews Molecular Cell Biology* (Vol. 9, Issue 1).

839 Cleveland, D. W., Mao, Y., & Sullivan, K. F., 2003. Centromeres and Kinetochores: From
840 Epigenetics to Mitotic Checkpoint Signaling. *Cell*, *112*(4), 407–421.

841 Colomina, N., Garí, E., Gallego, C., Herrero, E. and Aldea, M., 1999. G1 cyclins block the Ime1
842 pathway to make mitosis and meiosis incompatible in budding yeast. *The EMBO journal*, *18*(2),
843 pp.320-329.

844 Colomina, N., Liu, Y., Aldea, M. and Garí, E., 2003. TOR regulates the subcellular localization of
845 Ime1, a transcriptional activator of meiotic development in budding yeast. *Molecular and cellular*
846 *biology*, *23*(20), pp.7415-7424.

847 D'Ambrosio, C., Schmidt, C.K., Katou, Y., Kelly, G., Itoh, T., Shirahige, K. and Uhlmann, F.,
848 2008. Identification of cis-acting sites for condensin loading onto budding yeast
849 chromosomes. *Genes & development*, *22*(16), p.2215.

850 Dauban, L., Kamgoué, A., Wang, R., Léger-Silvestre, I., Beckouët, F., Cantaloube, S. and Gadal,
851 O., 2019. Quantification of the dynamic behaviour of ribosomal DNA genes and nucleolus during
852 yeast Saccharomyces cerevisiae cell cycle. *Journal of structural biology*, *208*(2), pp.152-164.

853 De Wulf, P., McAinsh, A. D., & Sorger, P. K., 2003. Hierarchical assembly of the budding yeast
854 kinetochore from multiple subcomplexes. *Genes and Development*, *17*(23).

855 Deng, X. and Kuo, M.H., 2018. Tripartite chromatin localization of budding yeast shugoshin
856 involves higher-ordered architecture of mitotic chromosomes. *G3: Genes, Genomes,*
857 *Genetics*, *8*(9), pp.2901-2911.

858 Dong, Q. and Li, F., 2022. Cell cycle control of kinetochore assembly. *Nucleus*, *13*(1), pp.210-
859 222.

860 Dou, Z., Liu, R., Zang, J., Yao, X. and Liu, X., 2023. The function, structure and dynamic
861 organization of centromeres and kinetochores. *JUSTC*, *53*, pp.1-9.

862 Fernius, J. and Hardwick, K.G., 2007. Bub1 kinase targets Sgo1 to ensure efficient chromosome
863 biorientation in budding yeast mitosis. *PLoS genetics*, *3*(11), p.e213.

864 Fernius, J. and Marston, A.L., 2009. Establishment of cohesion at the pericentromere by the Ctf19
865 kinetochore subcomplex and the replication fork-associated factor, Csm3. *PLoS genetics*, *5*(9),
866 p.e1000629.

867 Fischböck-Halwachs, J., Singh, S., Potocnjak, M., Hagemann, G., Solis-Mezarino, V., Woike, S.,
868 Ghodgaonkar-Steger, M., Weissmann, F., Gallego, L.D., Rojas, J. and Andreani, J., 2019. The
869 COMA complex interacts with Cse4 and positions Sli15/Ipl1 at the budding yeast inner
870 kinetochore. *Elife*, *8*, p.e42879.

871 Freeman, L., Aragon-Alcaide, L., & Strunnikov, A., 2000. The condensin complex governs
872 chromosome condensation and mitotic transmission of rDNA. *Journal of Cell Biology*, *149*(4).

873 Ghosh, S.K., Sau, S., Lahiri, S., Lohia, A. and Sinha, P., 2004. The Iml3 protein of the budding
874 yeast is required for the prevention of precocious sister chromatid separation in meiosis I and for
875 sister chromatid disjunction in meiosis II. *Current genetics*, *46*, pp.82-91.

876 Giet, R. and Glover, D.M., 2001. Drosophila aurora B kinase is required for histone H3
877 phosphorylation and condensin recruitment during chromosome condensation and to organize the
878 central spindle during cytokinesis. *The Journal of cell biology*, *152*(4), pp.669-682.

879 Glynn, E.F., Megee, P.C., Yu, H.G., Mistrot, C., Unal, E., Koshland, D.E., DeRisi, J.L. and Gerton,
880 J.L., 2004. Genome-wide mapping of the cohesin complex in the yeast Saccharomyces
881 cerevisiae. *PLoS biology*, *2*(9), p.e259.

882 Guacci, V., Koshland, D. and Strunnikov, A., 1997. A direct link between sister chromatid
883 cohesion and chromosome condensation revealed through the analysis of MCD1 in S.
884 cerevisiae. *Cell*, *91*(1), pp.47-57.

885 Güldener, U., Heck, S., Fiedler, T., Beinhauer, J. and Hegemann, J.H., 1996. A new efficient gene
886 disruption cassette for repeated use in budding yeast. *Nucleic acids research*, *24*(13), pp.2519-
887 2524.

888 Hadwiger, J. A., Wittenberg, C., Richardson, H. E., De Barros Lopes, M., & Reed, S. I. (1989). A
889 family of cyclin homologs that control the G1 phase in yeast). *Proceedings of the National*
890 *Academy of Sciences of the United States of America*, *86*(16).

891 Hinshaw, S.M., Makrantoni, V., Harrison, S.C. and Marston, A.L., 2017. The kinetochore receptor
892 for the cohesin loading complex. *Cell*, *171*(1), pp.72-84.

893 Hinshaw, S.M., Makrantoni, V., Kerr, A., Marston, A.L. and Harrison, S.C., 2015. Structural
894 evidence for Scc4-dependent localization of cohesin loading. *Elife*, *4*, p.e06057.

895 Jain, N., Janning, P. and Neumann, H., 2021. 14-3-3 Protein Bmh1 triggers short-range
896 compaction of mitotic chromosomes by recruiting sirtuin deacetylase Hst2. *Journal of Biological*
897 *Chemistry*, *296*.

898 Janke, C., Magiera, M.M., Rathfelder, N., Taxis, C., Reber, S., Maekawa, H., Moreno-Borchart,
899 A., Doenges, G., Schwob, E., Schiebel, E. and Knop, M., 2004. A versatile toolbox for PCR-based
900 tagging of yeast genes: new fluorescent proteins, more markers and promoter substitution
901 cassettes. *Yeast*, *21*(11), pp.947-962.

902 Kerr, G.W., Sarkar, S., Tibbles, K.L., Petronczki, M., Millar, J.B. and Arumugam, P., 2011.
903 Meiotic nuclear divisions in budding yeast require PP2ACdc55-mediated antagonism of Net1
904 phosphorylation by Cdk. *Journal of Cell Biology*, *193*(7), pp.1157-1166.

905 Kiburz, B.M., Reynolds, D.B., Megee, P.C., Marston, A.L., Lee, B.H., Lee, T.I., Levine, S.S.,
906 Young, R.A. and Amon, A., 2005. The core centromere and Sgo1 establish a 50-kb cohesin-
907 protected domain around centromeres during meiosis I. *Genes & development*, *19*(24), pp.3017-
908 3030.

909 Kim, S., Meyer, R., Chuong, H. and Dawson, D.S., 2013. Dual mechanisms prevent premature
910 chromosome segregation during meiosis. *Genes & development*, *27*(19), pp.2139-2146.

911 Kimura, K., Hirano, M., Kobayashi, R. and Hirano, T., 1998. Phosphorylation and activation of
912 13 S condensin by Cdc2 in vitro. *Science*, *282*(5388), pp.487-490.

913 Korns, J., Liu, X. and Takiar, V., 2022. A review of Plks: Thinking outside the (polo)
914 box. *Molecular Carcinogenesis*, *61*(2), pp.254-263.

915 Kruitwagen, T., Chymkowitch, P., Denoth-Lippuner, A., Enserink, J. and Barral, Y., 2018.
916 Centromeres license the mitotic condensation of yeast chromosome arms. *Cell*, *175*(3), pp.780-
917 795.

918 Kruitwagen, T., Denoth-Lippuner, A., Wilkins, B.J., Neumann, H. and Barral, Y., 2015. Axial
919 contraction and short-range compaction of chromatin synergistically promote mitotic chromosome
920 condensation. *Elife*, *4*, p.e10396.

921 Kumar, D., Prajapati, H.K., Mahilkar, A., Ma, C.H., Mittal, P., Jayaram, M. and Ghosh, S.K.,
922 2021. The selfish yeast plasmid utilizes the condensin complex and condensed chromatin for
923 faithful partitioning. *PLoS Genetics*, *17*(7), p.e1009660.

924 Lamothe, R., Costantino, L. and Koshland, D.E., 2020. The spatial regulation of condensin activity
925 in chromosome condensation. *Genes & Development*, *34*(11-12), pp.819-831.

926 Lavoie, B.D., Hogan, E. and Koshland, D., 2002. In vivo dissection of the chromosome
927 condensation machinery: reversibility of condensation distinguishes contributions of condensin
928 and cohesin. *The Journal of cell biology*, *156*(5), pp.805-815.

929 Lavoie, B.D., Hogan, E. and Koshland, D., 2004. In vivo requirements for rDNA chromosome
930 condensation reveal two cell-cycle-regulated pathways for mitotic chromosome folding. *Genes &*
931 *development*, *18*(1), pp.76-87.

932 Lee, B.H. and Amon, A., 2003. Role of Polo-like kinase CDC5 in programming meiosis I
933 chromosome segregation. *Science*, *300*(5618), pp.482-486.

934 Leonard, J., Sen, N., Torres, R., Sutani, T., Jarmuz, A., Shirahige, K. and Aragon, L., 2015.
935 Condensin relocalization from centromeres to chromosome arms promotes Top2 recruitment
936 during anaphase. *Cell Reports*, *13*(11), pp.2336-2344.

937 Li, P., Jin, H. and Yu, H.G., 2014. Condensin suppresses recombination and regulates double-
938 strand break processing at the repetitive ribosomal DNA array to ensure proper chromosome
939 segregation during meiosis in budding yeast. *Molecular biology of the cell*, *25*(19), pp.2934-2947.

940 Longtine, M.S., Mckenzie III, A., Demarini, D.J., Shah, N.G., Wach, A., Brachat, A., Philippsen,
941 P. and Pringle, J.R., 1998. Additional modules for versatile and economical PCR-based gene
942 deletion and modification in Saccharomyces cerevisiae. *Yeast*, *14*(10), pp.953-961.

943 Machín, F., Torres-Rosell, J., Jarmuz, A., & Aragón, L., 2005. Spindle-independent condensation-
944 mediated segregation of yeast ribosomal DNA in late anaphase. *Journal of Cell Biology*, *168*(2).

945 Makrantoni, V., Robertson, D. and Marston, A.L., 2019. Analysis of the chromosomal localization
946 of yeast SMC complexes by chromatin immunoprecipitation. *SMC Complexes: Methods and*
947 *Protocols*, pp.119-138.

948 Markowitz, T.E., Heldrich, J. and Hochwagen, A., 2020. DNA break formation induces
949 Scc2/cohesin-dependent recruitment of condensin to meiotic chromosomes. *bioRxiv*, pp.2020-07.

950 Mehta, G., Sanyal, K., Abhishek, S., Rajakumara, E. and Ghosh, S.K., 2022. Minichromosome
951 maintenance proteins in eukaryotic chromosome segregation. *BioEssays*, *44*(1), p.2100218.

952 Mehta, G.D., Agarwal, M. and Ghosh, S.K., 2014. Functional characterization of kinetochore
953 protein, Ctf19 in meiosis I: an implication of differential impact of Ctf19 on the assembly of
954 mitotic and meiotic kinetochores in Saccharomyces cerevisiae. *Molecular microbiology*, *91*(6),
955 pp.1179-1199.

956 Meraldi, P., McAinsh, A.D., Rheinbay, E. and Sorger, P.K., 2006. Phylogenetic and structural
957 analysis of centromeric DNA and kinetochore proteins. *Genome biology*, *7*, pp.1-21.

958 Meyer, R.E., Chuong, H.H., Hild, M., Hansen, C.L., Kinter, M. and Dawson, D.S., 2015.
959 Ipl1/Aurora-B is necessary for kinetochore restructuring in meiosis I in Saccharomyces
960 cerevisiae. *Molecular biology of the cell*, *26*(17), pp.2986-3000.

961 Michaelis, C., Ciosk, R. and Nasmyth, K., 1997. Cohesins: chromosomal proteins that prevent
962 premature separation of sister chromatids. *Cell*, *91*(1), pp.35-45.

963 Mishra, P.K., Ciftci-Yilmaz, S., Reynolds, D., Au, W.C., Boeckmann, L., Dittman, L.E., Jowhar,
964 Z., Pachpor, T., Yeh, E., Baker, R.E. and Hoyt, M.A., 2016. Polo kinase Cdc5 associates with
965 centromeres to facilitate the removal of centromeric cohesin during mitosis. *Molecular Biology of*
966 *the Cell*, *27*(14), pp.2286-2300.

967 Mishra, P.K., Olafsson, G., Boeckmann, L., Westlake, T.J., Jowhar, Z.M., Dittman, L.E., Baker,
968 R.E., D'Amours, D., Thorpe, P.H. and Basrai, M.A., 2019. Cell cycle–dependent association of
969 polo kinase Cdc5 with CENP-A contributes to faithful chromosome segregation in budding
970 yeast. *Molecular Biology of the Cell*, *30*(8), pp.1020-1036.

971 Mittal, P., Ghule, K., Trakroo, D., Prajapati, H. K., & Ghosh, S. K., 2020. Meiosis-Specific
972 Functions of Kinesin Motors in Cohesin Removal and Maintenance of Chromosome Integrity in
973 Budding Yeast. *Molecular and Cellular Biology*, *40*(8).

974 Mora-Bermúdez, F., Gerlich, D. and Ellenberg, J., 2007. Maximal chromosome compaction occurs
975 by axial shortening in anaphase and depends on Aurora kinase. *Nature cell biology*, *9*(7), pp.822-
976 831.

977 Müller, C.A. and Nieduszynski, C.A., 2012. Conservation of replication timing reveals global and
978 local regulation of replication origin activity. *Genome research*, *22*(10), pp.1953-1962.

979 Nakazawa, N., Nakamura, T., Kokubu, A., Ebe, M., Nagao, K. and Yanagida, M., 2008. Dissection
980 of the essential steps for condensin accumulation at kinetochores and rDNAs during fission yeast
981 mitosis. *The Journal of cell biology*, *180*(6), pp.1115-1131.

982 Natsume, T., Müller, C.A., Katou, Y., Retkute, R., Gierliński, M., Araki, H., Blow, J.J., Shirahige,
983 K., Nieduszynski, C.A. and Tanaka, T.U., 2013. Kinetochores coordinate pericentromeric
984 cohesion and early DNA replication by Cdc7-Dbf4 kinase recruitment. *Molecular cell*, *50*(5),
985 pp.661-674.

986 Nishimura, K., Fukagawa, T., Takisawa, H., Kakimoto, T. and Kanemaki, M., 2009. An auxin-
987 based degron system for the rapid depletion of proteins in nonplant cells. *Nature methods*, *6*(12),
988 pp.917-922.

989 Oelschlaegel, T., Schwickart, M., Matos, J., Bogdanova, A., Camasses, A., Havlis, J., Shevchenko,
990 A. and Zachariae, W., 2005. The yeast APC/C subunit Mnd2 prevents premature sister chromatid
991 separation triggered by the meiosis-specific APC/C-Ama1. *Cell*, *120*(6), pp.773-788.

992 Okaz, E., Argüello-Miranda, O., Bogdanova, A., Vinod, P.K., Lipp, J.J., Markova, Z., Zagoriy, I.,
993 Novak, B. and Zachariae, W., 2012. Meiotic prophase requires proteolysis of M phase regulators
994 mediated by the meiosis-specific APC/CAma1. *Cell*, *151*(3), pp.603-618.

995 Ontoso, D., Acosta, I., van Leeuwen, F., Freire, R. and San-Segundo, P.A., 2013. Dot1-dependent
996 histone H3K79 methylation promotes activation of the Mek1 meiotic checkpoint effector kinase
997 by regulating the Hop1 adaptor. *PLoS genetics*, *9*(1), p.e1003262.

998 Peplowska, K., Wallek, A.U. and Storchova, Z., 2014. Sgo1 regulates both condensin and
999 Ipl1/Aurora B to promote chromosome biorientation. *PLoS Genetics*, *10*(6), p.e1004411.

1000 Petersen, J. and Hagan, I.M., 2003. S. pombe aurora kinase/survivin is required for chromosome
1001 condensation and the spindle checkpoint attachment response. *Current biology*, *13*(7), pp.590-
1002 597.

1003 Piazza, I., Rutkowska, A., Ori, A., Walczak, M., Metz, J., Pelechano, V., Beck, M. and Haering,
1004 C.H., 2014. Association of condensin with chromosomes depends on DNA binding by its HEAT-
1005 repeat subunits. *Nature structural & molecular biology*, *21*(6), pp.560-568.

1006 Shah, S., Mittal, P., Kumar, D., Mittal, A., & Ghosh, S. K., 2023. Evidence of kinesin motors
1007 involved in stable kinetochore assembly during early meiosis. *Molecular Biology of the Cell*,
1008 *34*(11).

1009 Shirk, K., Jin, H., Giddings Jr, T.H., Winey, M. and Yu, H.G., 2011. The Aurora kinase Ipl1 is
1010 necessary for spindle pole body cohesion during budding yeast meiosis. *Journal of cell*
1011 *science*, *124*(17), pp.2891-2896.

1012 Snead, J.L., Sullivan, M., Lowery, D.M., Cohen, M.S., Zhang, C., Randle, D.H., Taunton, J.,
1013 Yaffe, M.B., Morgan, D.O. and Shokat, K.M., 2007. A coupled chemical-genetic and

1014 bioinformatic approach to Polo-like kinase pathway exploration. *Chemistry & biology*, *14*(11),
1015 pp.1261-1272.

1016 Song, S., Grenfell, T. Z., Garfield, S., Erikson, R. L., & Lee, K. S., 2000. Essential Function of the
1017 Polo Box of Cdc5 in Subcellular Localization and Induction of Cytokinetic Structures. *Molecular*
1018 *and Cellular Biology*, *20*(1).

1019 St-Pierre, J., Douziech, M., Bazile, F., Pascariu, M., Bonneil, É., Sauvé, V., Ratsima, H. and
1020 D'Amours, D., 2009. Polo kinase regulates mitotic chromosome condensation by hyperactivation
1021 of condensin DNA supercoiling activity. *Molecular cell*, *34*(4), pp.416-426.

1022 Strunnikov, A. V., Hogan, E., & Koshland, D., 1995. SMC2, a Saccharomyces cerevisiae gene
1023 essential for chromosome segregation and condensation, defines a subgroup within the SMC
1024 family. *Genes and Development*, *9*(5).

1025 Sutani, T., Yuasa, T., Tomonaga, T., Dohmae, N., Takio, K. and Yanagida, M., 1999. Fission yeast
1026 condensin complex: essential roles of non-SMC subunits for condensation and Cdc2
1027 phosphorylation of Cut3/SMC4. *Genes & development*, *13*(17), pp.2271-2283.

1028 Takai, N., Hamanaka, R., Yoshimatsu, J. and Miyakawa, I., 2005. Polo-like kinases (Plks) and
1029 cancer. *Oncogene*, *24*(2), pp.287-291.

1030 Takemoto, A., Murayama, A., Katano, M., Urano, T., Furukawa, K., Yokoyama, S., Yanagisawa,
1031 J., Hanaoka, F. and Kimura, K., 2007. Analysis of the role of Aurora B on the chromosomal
1032 targeting of condensin I. *Nucleic acids research*, *35*(7), pp.2403-2412.

1033 Tanaka, T., Fuchs, J., Loidl, J. and Nasmyth, K., 2000. Cohesin ensures bipolar attachment of
1034 microtubules to sister centromeres and resists their precocious separation. *Nature cell*
1035 *biology*, *2*(8), pp.492-499.

1036 Torres-Rosell, J., Machín, F., Jarmuz, A., & Aragón, L., 2004. Nucleolar segregation lags behind
1037 the rest of the genome and requires Cdc14 phosphatase activation by the FEAR network. *Cell*
1038 *Cycle*, *3*(4).

1039 Tsubouchi, T. and Roeder, G.S., 2005. A synaptonemal complex protein promotes homology-
1040 independent centromere coupling. *Science*, *308*(5723), pp.870-873.

1041 Tsuchiya, D., Yang, Y., & Lacefield, S., 2014. Positive Feedback of NDT80 Expression Ensures
1042 Irreversible Meiotic Commitment in Budding Yeast. *PLoS Genetics*, *10*(6).

1043 Vas, A.C., Andrews, C.A., Kirkland Matesky, K. and Clarke, D.J., 2007. In vivo analysis of
1044 chromosome condensation in Saccharomyces cerevisiae. *Molecular biology of the cell*, *18*(2),
1045 pp.557-568.

1046 Verzijlbergen, K.F., Nerusheva, O.O., Kelly, D., Kerr, A., Clift, D., de Lima Alves, F., Rappsilber,
1047 J. and Marston, A.L., 2014. Shugoshin biases chromosomes for biorientation through condensin
1048 recruitment to the pericentromere. *Elife*, *3*, p.e01374.

1049 Wach, A., 1996. PCR-synthesis of marker cassettes with long flanking homology regions for gene
1050 disruptions in S. cerevisiae. *Yeast*, *12*(3), pp.259-265.

1051 Walters, A.D., May, C.K., Dauster, E.S., Cinquin, B.P., Smith, E.A., Robellet, X., D'Amours, D.,
1052 Larabell, C.A. and Cohen-Fix, O., 2014. The yeast polo kinase Cdc5 regulates the shape of the
1053 mitotic nucleus. *Current Biology*, *24*(23), pp.2861-2867.

1054 Westermann, S., Drubin, D. G., & Barnes, G., 2007. Structures and functions of yeast kinetochore
1055 complexes. In *Annual Review of Biochemistry* (Vol. 76).

1056 Wilkins, B.J., Rall, N.A., Ostwal, Y., Kruitwagen, T., Hiragami-Hamada, K., Winkler, M., Barral,
1057 Y., Fischle, W. and Neumann, H., 2014. A cascade of histone modifications induces chromatin
1058 condensation in mitosis. *Science*, *343*(6166), pp.77-80.

1059 Wong, J., Nakajima, Y., Westermann, S., Shang, C., Kang, J.S., Goodner, C., Houshmand, P.,
1060 Fields, S., Chan, C.S., Drubin, D. and Barnes, G., 2007. A protein interaction map of the mitotic
1061 spindle. *Molecular biology of the cell*, *18*(10), pp.3800-3809.

1062 Yahya, G., Wu, Y., Peplowska, K., Röhrl, J., Soh, Y.M., Bürmann, F., Gruber, S. and Storchova,
1063 Z., 2020. Phospho-regulation of the Shugoshin-Condensin interaction at the centromere in budding
1064 yeast. *PLoS genetics*, *16*(8), p.e1008569.

1065 Yamin, K., Assa, M., Matityahu, A., and Onn, I., 2020. Analyzing chromosome condensation in
1066 yeast by second-harmonic generation microscopy. *Current Genetics, 66*(2), 437–443. doi:
1067 10.1007/s00294-019-01034-1

1068 Yamin, K., Bijlani, S., Berman, J., Soni, A., Shlomai, J., Buragohain, B. M., and Onn, I., 2022.
1069 Fold-change of chromatin condensation in yeast is a conserved property. *Scientific Reports, 12*(1),
1070 17393. doi: 10.1038/s41598-022-22340-8

1071 Yu, H.G. and Koshland, D., 2005. Chromosome morphogenesis: condensin-dependent cohesin
1072 removal during meiosis. *Cell*, *123*(3), pp.397-407.

1073 Zeng, X., Kahana, J.A., Silver, P.A., Morphew, M.K., McIntosh, J.R., Fitch, I.T., Carbon, J. and
1074 Saunders, W.S., 1999. Slk19p is a centromere protein that functions to stabilize mitotic
1075 spindles. *The Journal of cell biology*, *146*(2), pp.415-425.

1076 Zoller, J.F., Herrmann, R.G. and Wanner, G., 2004. Chromosome condensation in mitosis and
1077 meiosis of rye (Secale cereale L.). *Cytogenetic and Genome Research*, *105*(1), pp.134-144.

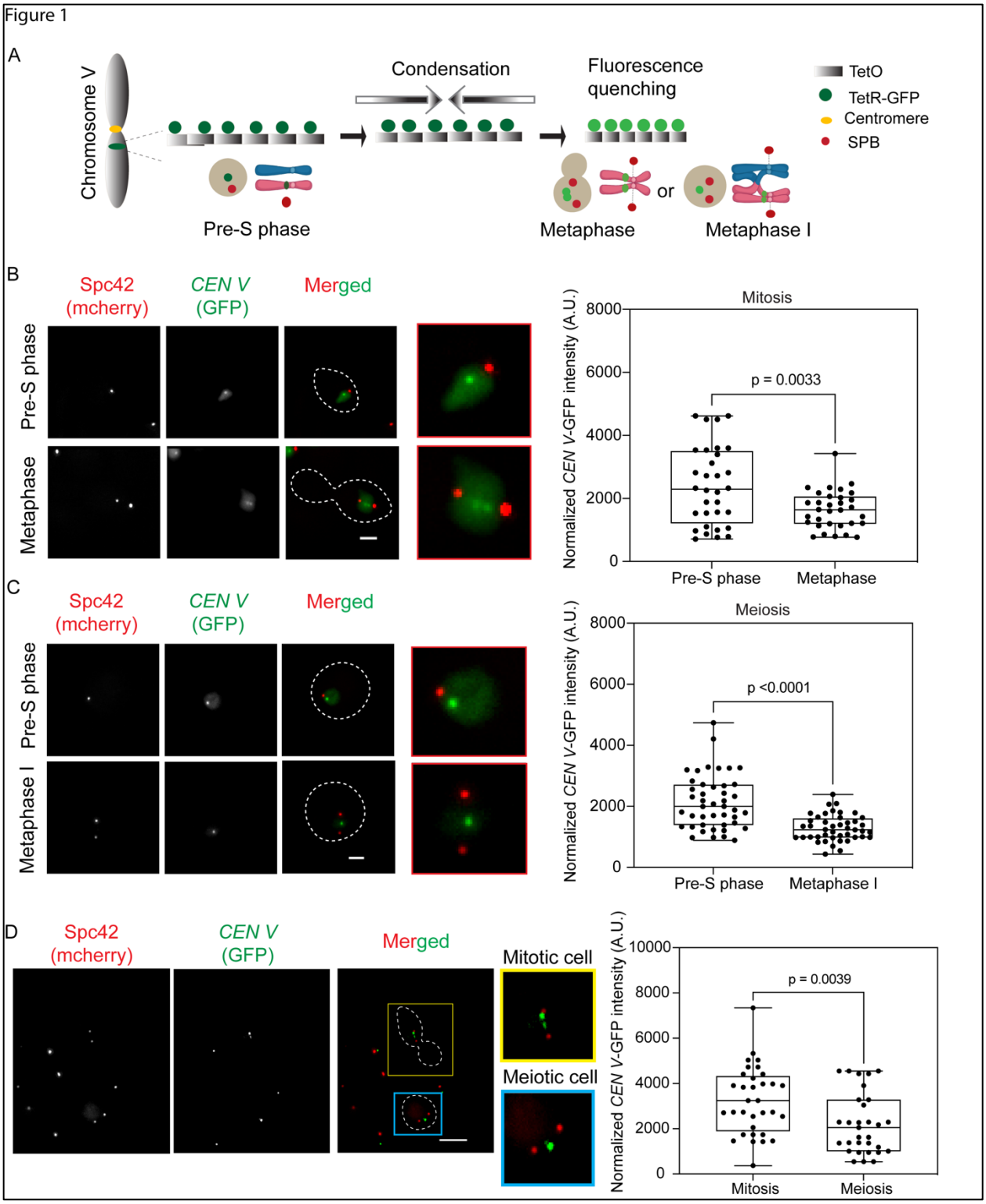

Figure 1. Chromosomes are more condensed in meiosis than in mitosis. (A) Schematic diagrams showing the strategy adopted for in vivo measurement of chromosome condensation. One copy of chromosome V was tagged using $[TetO]_{224}$-[TetR-GFP] system near the centromere V. As the $[TetO]_{224}$ repeats come closer due to axial condensation in the metaphase stage, the GFP signal intensity decreases

1083 because of fluorescence quenching. The fluorescence intensity of *CEN V*-GFP measured in (B) mitotic and
1084 (C) meiotic cells (see materials methods for detail) from the indicated cell cycle stages in the wild type
1085 (SGY9012) are graphically represented on the right; the corresponding representative images are shown on
1086 the left. N ≥ 30-45 from three independent experiments, scale bar = 2 µm. (D) The cells used in (B) and (C)
1087 were mixed and fluorescence intensity was measured from mitotic (budded), and meiotic (unbudded) cells
1088 present in the same field of view as represented on the left; the fluorescence intensities are presented
1089 graphically on right. N ≥ 30 from two independent experiments, scale bar = 5 µm. The intensity values were
1090 normalized with background intensities. For statistical significance, *p* values were estimated by the two-
1091 tailed student's t-test for the mean.

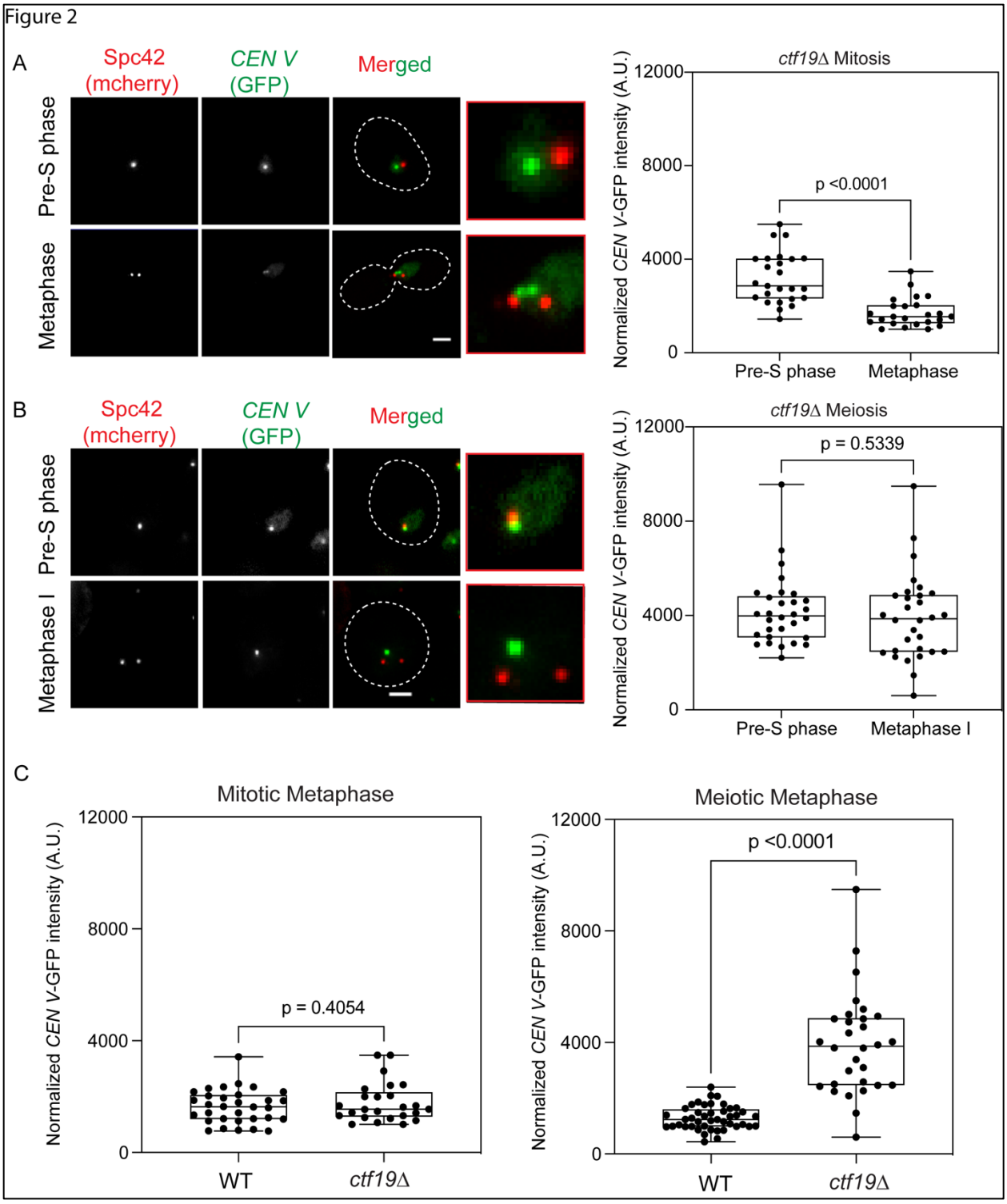

1092

1093 **Figure 2. Ctf19 is involved in chromosome condensation in meiosis but not in mitosis.** In vivo,
1094 chromosome condensation in *ctf19*Δ cells (SGY9019) was measured as in Fig. 1 at the indicated stages in
1095 mitosis (A) and in meiosis (B). (C) The fluorescence intensity of *CEN V*-GFP measured for both the wild
1096 type (SGY9012) and *ctf19*Δ (SGY9019) cells in the mitotic metaphase stage (left) and meiotic metaphase
1097 stage (right) are graphically represented. N = 25-30 from two independent experiments. Error bars represent

1098 the standard deviation from the mean values obtained from two- three independent experiments. For
1099 statistical significance, *p* values were estimated by the two-tailed student's t-test for the mean.

1100

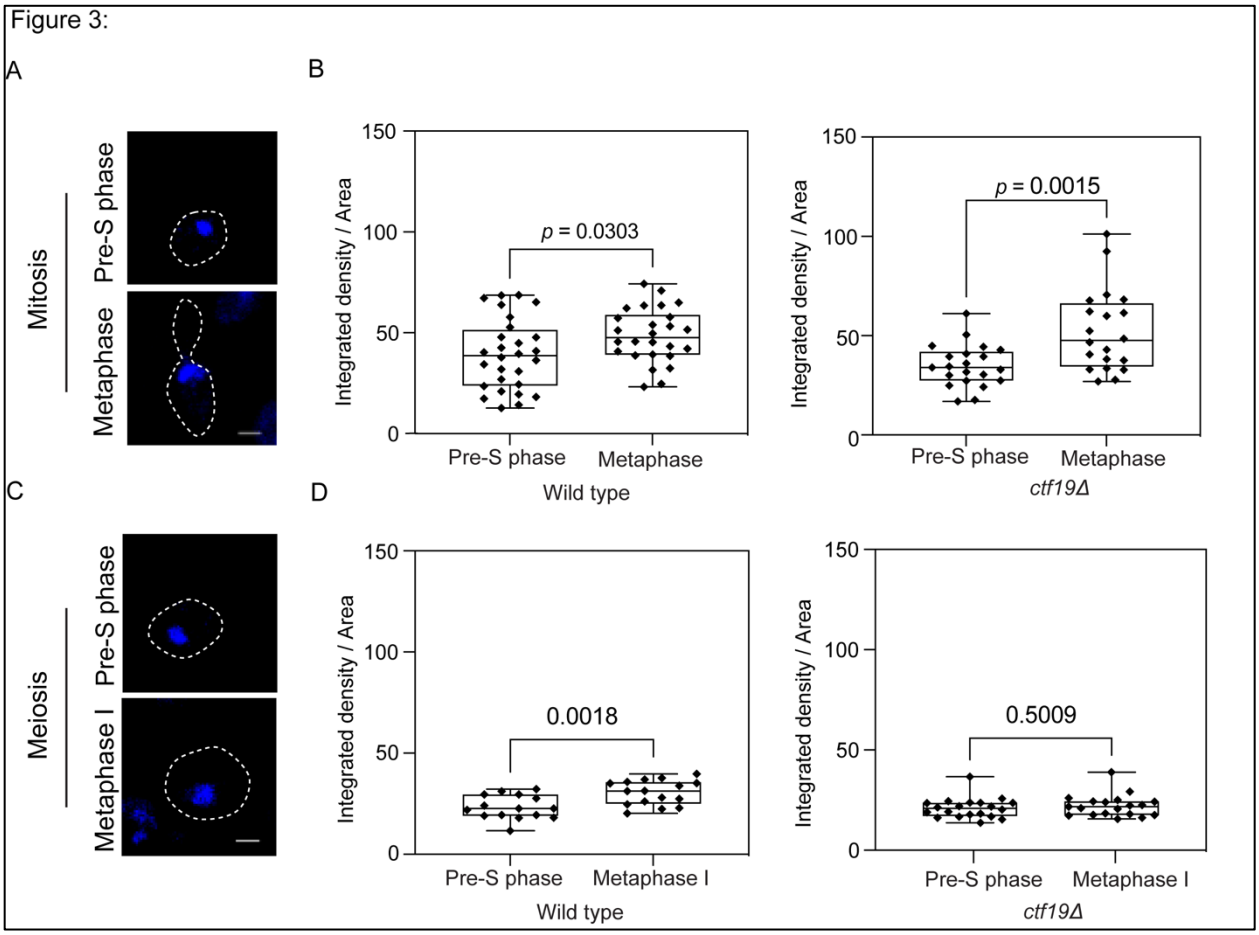

1101

1102 **Figure 3**. **The loss of Ctf19 leads to meiotic specific chromosome condensation defect.** (A) Analysis of
1103 condensation of the chromosomes stained with DAPI in wild type (SGY9012) and *ctf19*Δ (SGY9019) mitotic
1104 cells by Second Harmonic Generation (SHG) microscopy. Cells in the mitotic pre-S phase or metaphase were
1105 selected based on bud morphology and DAPI position within the cell. (B) Box plot showing the integrated
1106 density/area from pre-S phase cells and M phase cells after analysis using Image J for the indicated strains.
1107 (C) Similar analysis as in A for the meiotic cells. Cells in meiotic pre-S phase or metaphase I were collected
1108 at different time points following their release into SPM as mentioned in Fig S1 (see materials and methods).
1109 (D) Similar graphs as in B for the meiotic cells. Representative images show the areas taken for analysis after
1110 two-photon excitation in SHG microscopy.

1111

1112

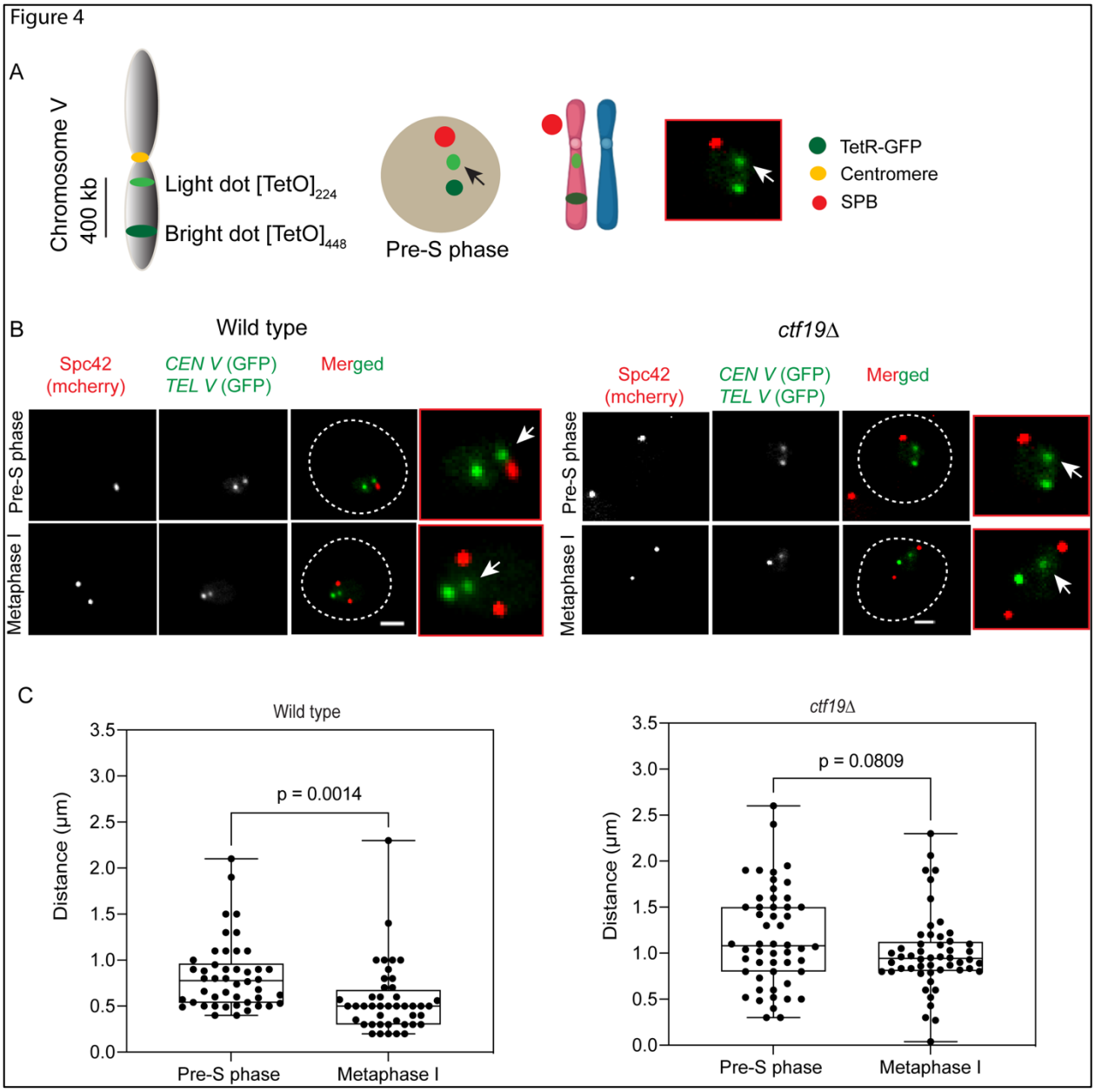

Figure 4. Ctf19 contributes to chromosome condensation along the chromosomal arm (A) One copy of chromosome V was marked with GFP at two different chromosomal loci ~400 kb away from each other, each proximal to the centromere or telomere was marked with $[TetO]_{224}$–[TetR-GFP] as *CEN V*-GFP or with $[TetO]_{448}$ –[TetR-GFP] as *TEL V*-GFP, respectively. The *TEL V*-GFP dot appeared brighter than the *CEN V*-GFP dot (arrow). (B) The representative images are shown for the indicated strains (wild type: SGY9092, *ctf19Δ*: SGY9124) and the cell cycle stages. Scale bar = 2 µm. (C) The 3D distances between the *CEN V*-GFP and *TEL V*-GFP dots measured as described in the materials and methods are shown for the wild type (left) and *ctf19*Δ (right) strains used in B harvested from the indicated cell cycle stages. N = 45-50 from two independent experiments. The statistical significance *p* value was estimated by the two-tailed student's t-test for the mean.

1124

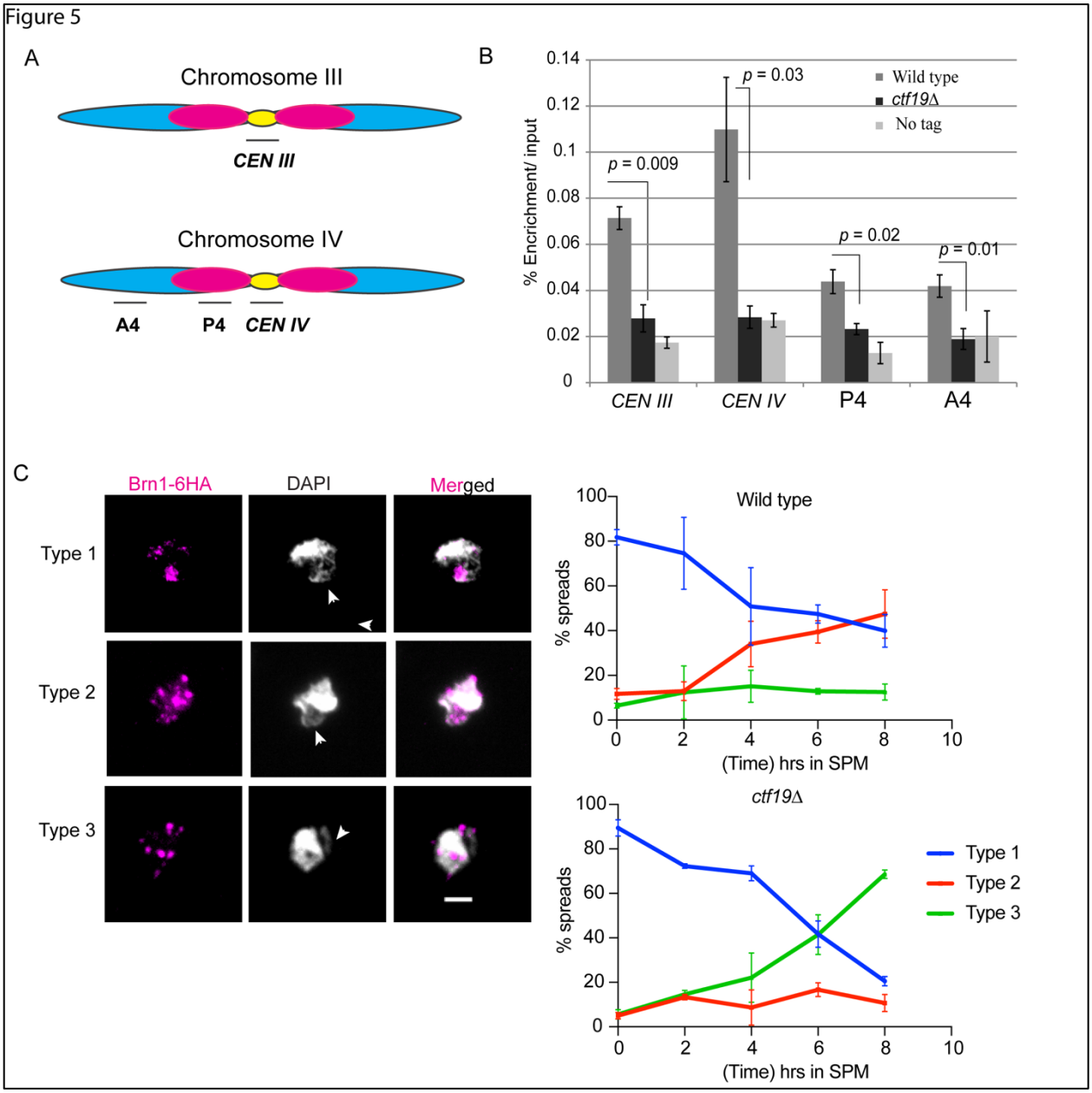

1125

1126 **Figure 5. The loss of Ctf19 causes reduced association of condensin with chromatin by impairing the**
1127 **establishment of the association in meiosis** (A) Schematic diagram showing the locations of PCR
1128 amplicons (horizontal bars) on chromosomes III and IV used for the qPCR analysis of the ChIP samples.
1129 The yellow oval shapes represent the centromeres (*CEN III* and *CEN IV*), pink and blue regions indicate the
1130 pericentromeric (P) and arm (A) regions, respectively. (B) ChIP assay using anti-HA antibodies (3F10) for
1131 quantifying the association of Brn1-6HA with the indicated chromosomal loci in the wild type (SGY283)
1132 and *ctf19*Δ (SGY284) cells arrested at metaphase I. The graph represents % enrichment per input obtained
1133 by qPCR analysis. Error bars represent the standard deviation from the mean values obtained from three

independent experiments. The statistical significance *p* value was estimated by the two-tailed student's t-test for the mean. (C) The loss of Ctf19 impairs the establishment of the association of condensin with chromatin in meiosis. The left panel shows the representative images of the chromatin spreads showing different types of association (described in the text) of the condensin subunit (Brn1-6HA) with chromatin at different time points in SPM in strains used in B harboring homozygous *BRN1-6HA* allele. Types 1 – 2 are categorized as localization of Brn1-6HA first at rDNA (type 1) and then gradually spreading to rest of the chromatin (type 2). Type 3 implies a gross reduction in chromatin-condensin association. Anti-HA antibodies (3F10) were used to detect Brn1-6HA. The right panel represents the percentage of different types of spreads at the indicated time points. with respect to the Brn1-6HA signal. Arrowhead shows rDNA region. N >100 from two independent experiments, scale bar = 2 µm.

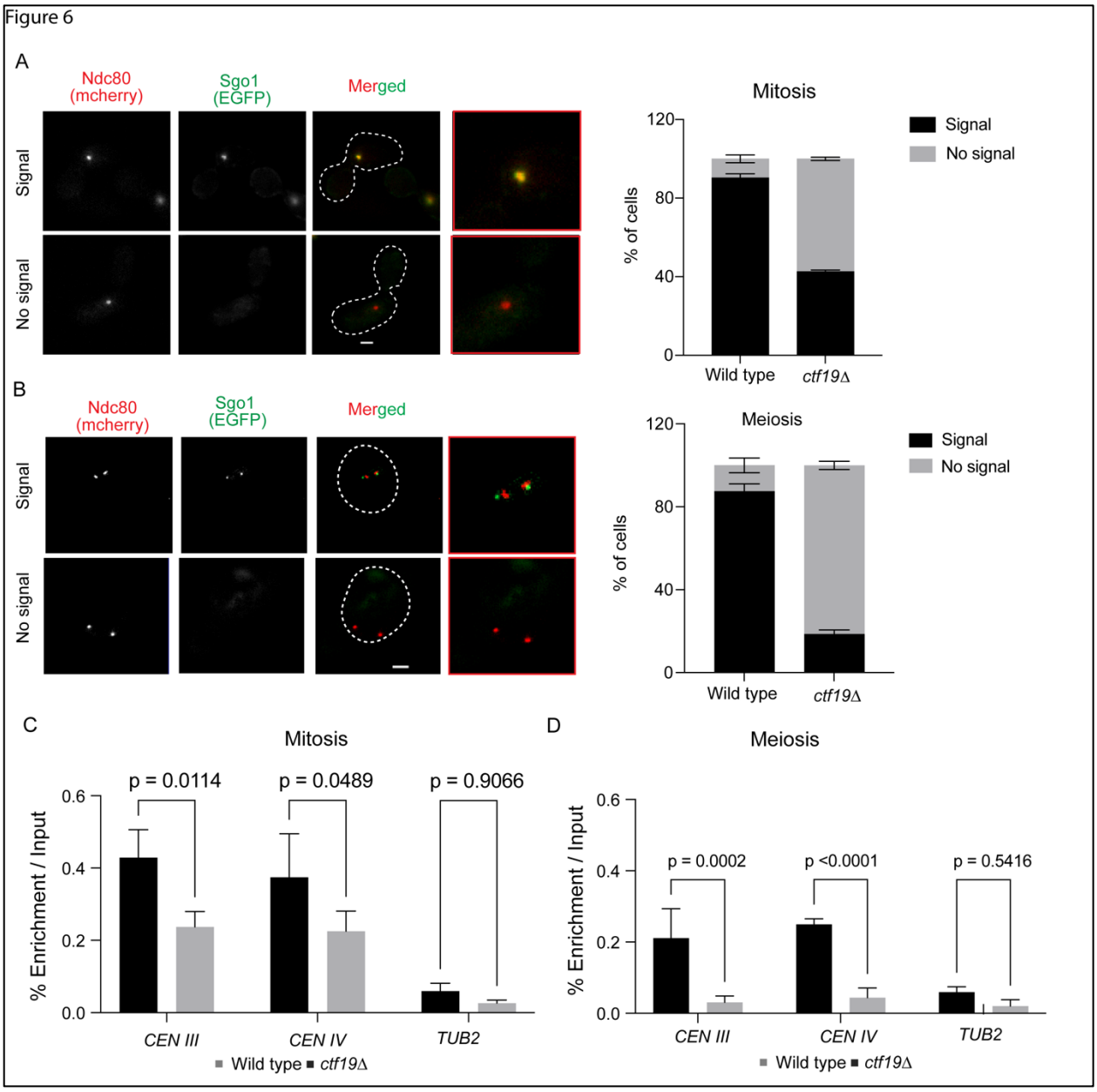

1145 **Figure 6. Pericentric localization of Sgo1 is perturbed in the *ctf19Δ* cells compared to the wild type**
1146 **more in meiosis than in mitosis.** The localization of Sgo1-GFP with respect to a kinetochore protein,
1147 Ndc80-mCherry in the wild type (SGY9189) and *ctf19Δ* (SGY9193) cells arrested at metaphase upon
1148 treatment with nocodazole (A) and harvested at metaphase I following their release into SPM for 8 and 10
1149 hrs (B), respectively. The left panel shows the representative images of indicated categories and the right
1150 panel depicts the percentage of cells in each category. Error bars represent the standard deviation from the
1151 mean values obtained from two independent experiments. N = 90-120, scale bar = 2 µm. ChIP assays using
1152 anti-Myc antibodies (ab9106) for quantifying association of Sgo1-9Myc with the indicated chromosomal
1153 loci in the wild type (SGY9194) and *ctf19*Δ (SGY9195) cells arrested at metaphase (C) and metaphase I
1154 (D), as in (A) and (B). The graph represents % enrichment per input obtained by qPCR analysis. Error bars
1155 represent the standard deviation from the mean values obtained from three independent experiments. The
1156 statistical significance *p* value was estimated by the two-tailed student's t-test for the mean.

1157

Figure 7

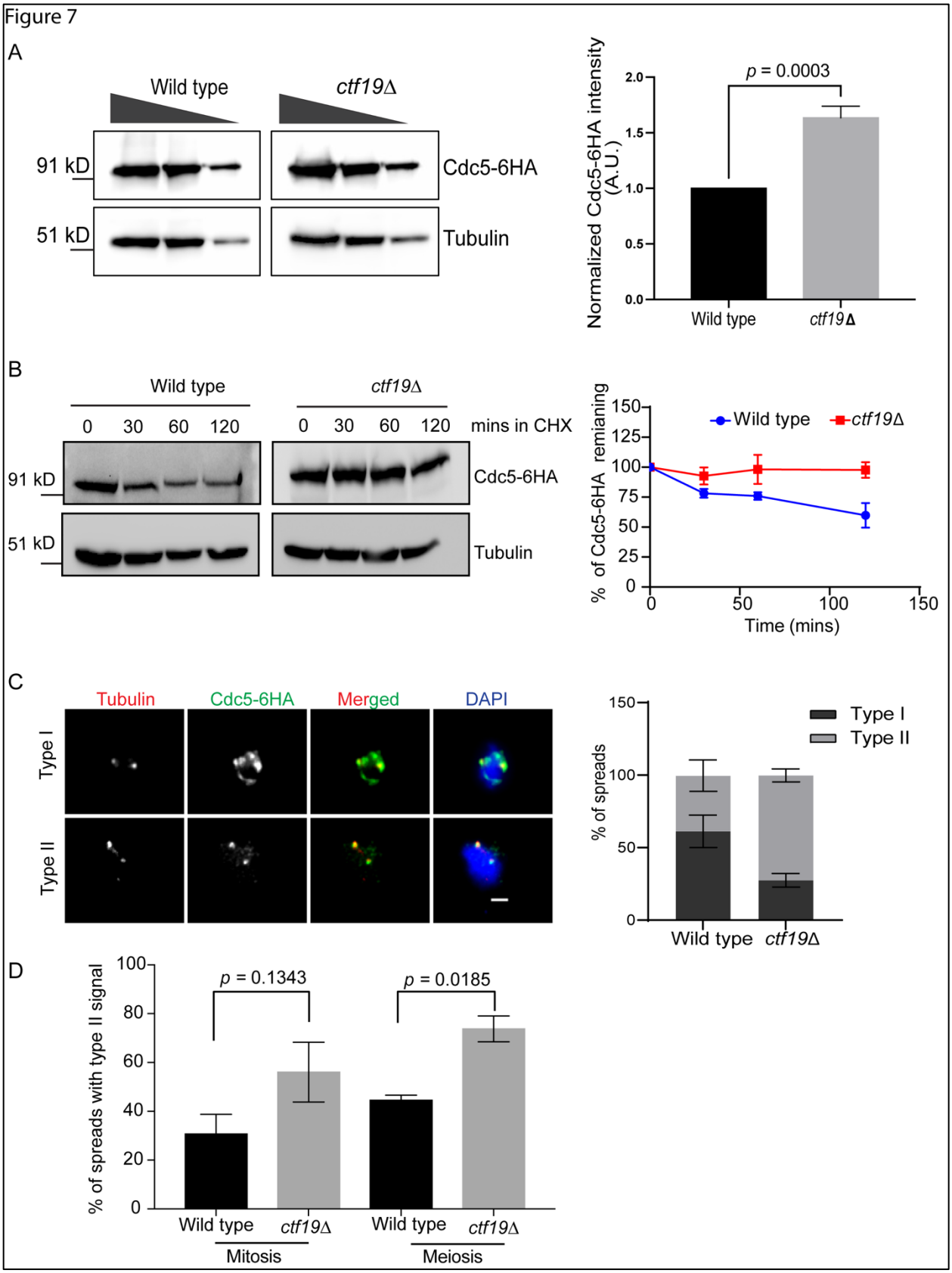

1158

1159 **Figure 7. Increase in the level of Cdc5 and decrease in its chromatin association in *ctf19Δ* mutant in**
1160 **meiosis**. (A) The wild type (SGY9152) and *ctf19Δ* (SGY9148) cells harboring *CDC5-6HA pCLB2-CDC20*
1161 were arrested at the metaphase I following 8 and 10 hrs of meiotic induction, respectively. Left, the proteins
1162 extracted from the cells were run on a gel in dilutions and were detected by western blotting using anti-HA
1163 (3F10) and anti-tubulin (YOL1/34) antibodies. Right, the intensity of the bands was calculated using ImageJ
1164 software and normalized to the tubulin band intensity used as loading control. *p* value was estimated by the
1165 two-tailed student's t-test for the mean (B) Cdc5-6HA stability in wild type (SGY9139) and *ctf19*Δ
1166 (SGY9140) cells. Following release into synchronized meiosis for 8 and 10 hrs for the wild type and the
1167 mutant, respectively, the cells were treated with CHX (t = 0). The cells were harvested at indicated time
1168 points. Cdc5-6HA and tubulin levels were analyzed by western blotting (*left*) as in (A) and quantified (*right*)
1169 at indicated time points after CHX treatment. Error bars represent the standard deviation from the mean
1170 values obtained from three independent experiments. (C) Left, the representative images of the chromatin
1171 spreads show the association of Cdc5-6HA with chromatin in metaphase I arrested wild type and *ctf19Δ*
1172 strains as used in A harboring homozygous *CDC5-6HA* alleles. Right, quantitative analysis of Cdc5-6HA
1173 signal (*right*) on the chromatin spreads as type I (bright signal) and type II (low signal) categories. The
1174 metaphase I stage of the spreads was determined by SPB localization revealed by tubulin immunostaining.
1175 (D) The percentage of chromatin spreads with type II signal, as mentioned in (C), from the cells arrested in
1176 metaphase (mitosis) by Cdc20 degradation (materials and methods) or metaphase I (meiosis). Error bars
1177 represent the standard deviation from the mean values obtained from two independent experiments (N =
1178 83, scale bar = 2 μm).

1179

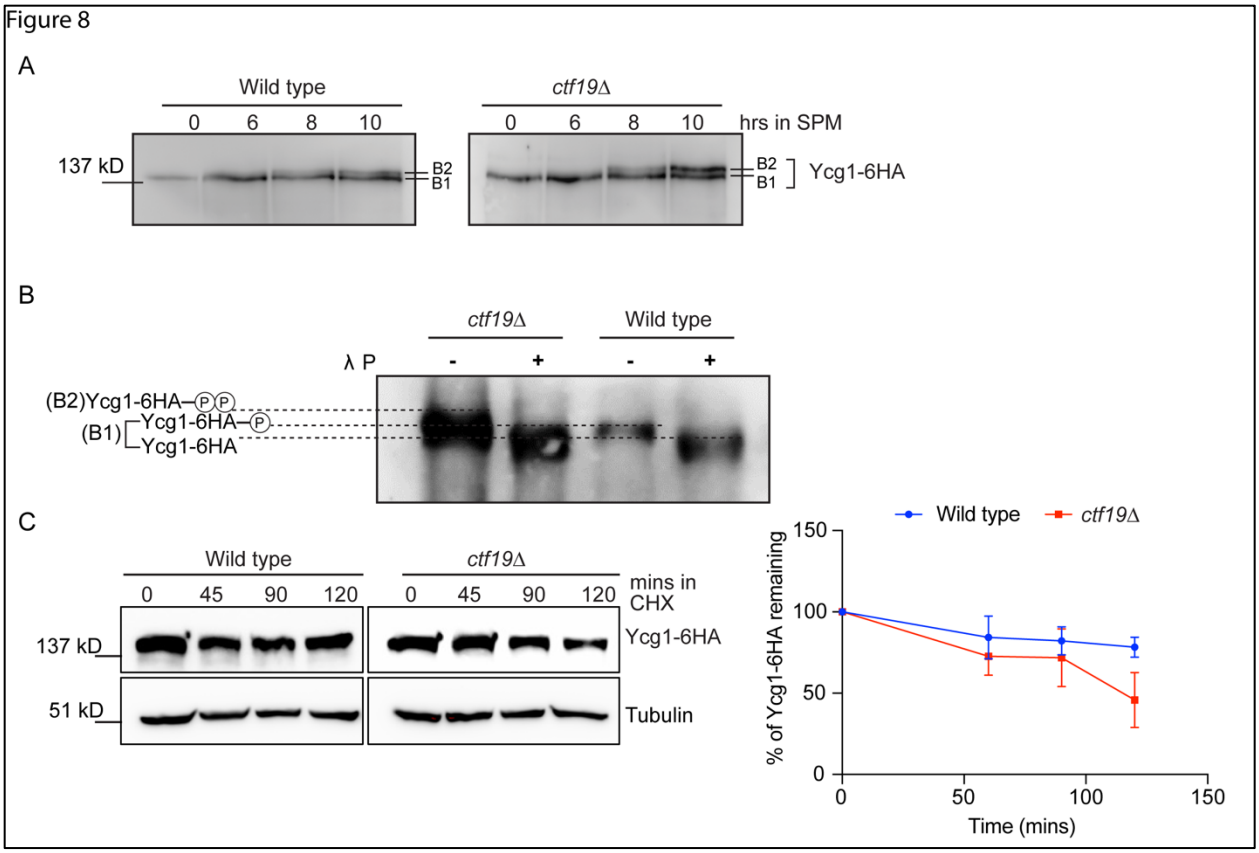

Figure 8. Evidence of hyper-phosphorylation and reduced stability of Ycg1 in *ctf19* mutant in meiosis. (A) The wild type (SGY9232) and *ctf19Δ* (SGY9233) cells harboring *YCG1-6HA pCLB2-CDC20* were released into synchronized meiosis and were harvested at the indicated time points; proteins extracted by the TCA method (materials and methods) from the cells were resolved by running 6% SDS-PAGE gel and were detected by western blotting using anti-HA antibodies (12CA5). Notably, the B2 band is more prominent than the B1 band in the mutant. (B) The wild type and *ctf19Δ* strains used in A harboring *YCG1-6HA pCLB2-CDC20* were released into SPM and the samples were harvested at 8 hrs and 10 hrs, respectively. Protein extracts treated with (+) or without (-) lambda phosphatase (λ P) were run on 7.5% SDS gel made with Phos-tag acrylamide (Wako) to detect Ycg1-6HA by western blotting using anti-HA antibodies (12CA5). (C) Ycg1-6HA stability in wild type and *ctf19*Δ cells. The cells were treated with CHX (t = 0) following 8 and 10 hrs into meiotic induction for the wild type and *ctf19Δ*, respectively. Left, the protein extracts were resolved on 10% SDS-PAGE gel and the protein level was analyzed by western blotting using anti-HA (12CA5) and anti-tubulin (YOL1/34) antibodies in the cells harvested at indicated time points. Right, quantification of Ycg1-6HA bands normalized with the tubulin bands using ImageJ software at indicated time points after CHX treatment. Error bars represent the standard deviation from the mean values obtained from two independent experiments.

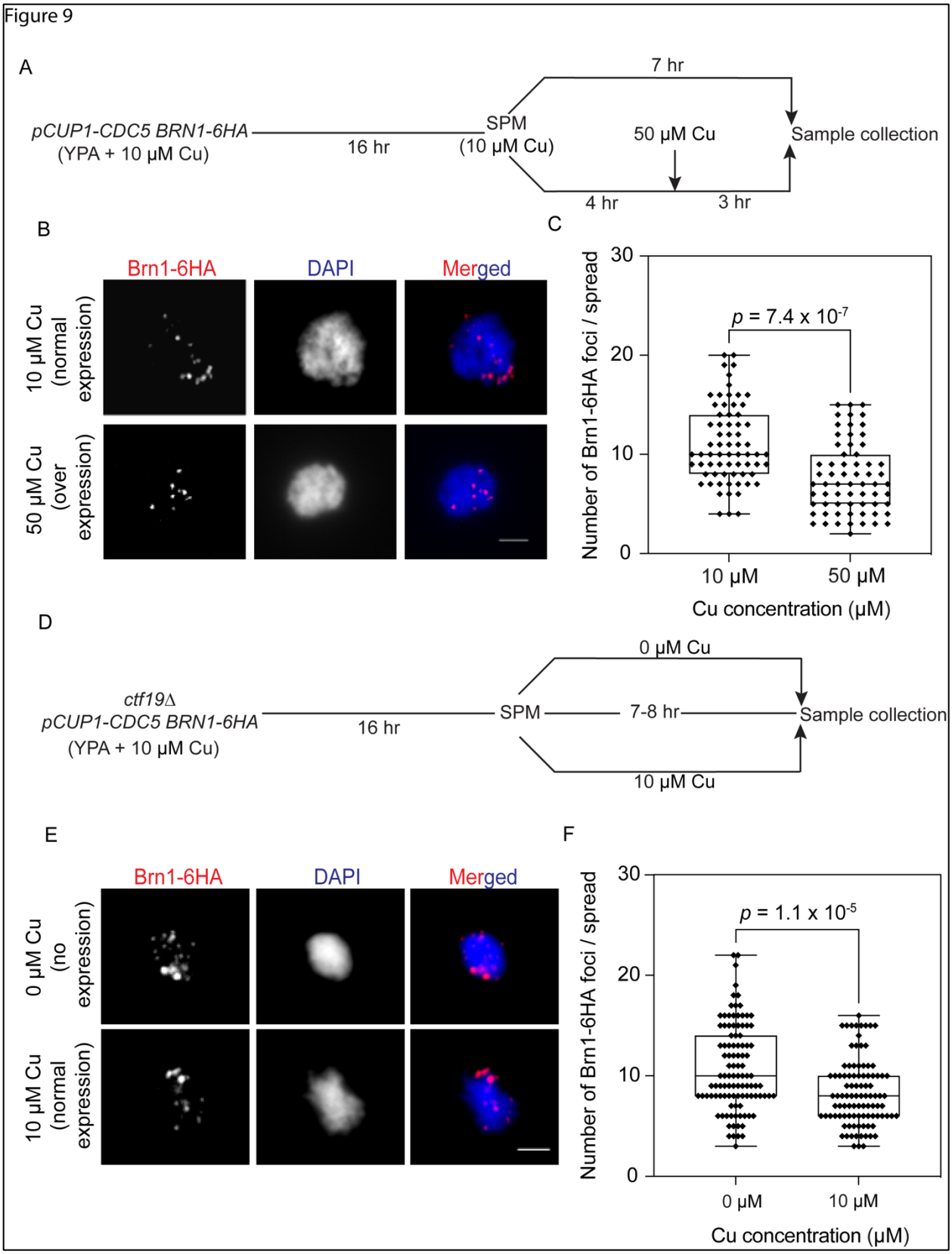

1198

1199 **Figure 9. Misregulation of Cdc5 influences chromatin-condensin association.** (A) Schematic
1200 representation of the experimental strategy. Wild type cells (SGY18007) with homozygous *pCUP1-CDC5*

1201 and *BRN1-6HA* alleles were grown in YPA supplemented with 10 μM copper used for normal expression
1202 of *CDC5.* The cells were released into SPM supplemented with either 10 μM or 50 μM (used for over
1203 expression of *CDC5*) copper, respectively. The samples were harvested at the indicated time point for
1204 analysis by chromatin spread assay. (B) Representative images of the chromatin spreads showing
1205 chromatin-Brn1-6HA association under normal or overexpression of *CDC5* in the wild type cells. Anti-HA
1206 antibody (3F10) was used to detect Brn1-6HA. (C) Box plots showing the number of Brn1-6HA foci per
1207 nuclear spread of the wild type cells. N = 60 from two independent experiments. (D, E, F) Same as in A, B
1208 and C, respectively except *ctf19*Δ cells (SGY18015) and 0 μM copper was used instead of wild type cells
1209 and 50 μM copper, respectively. For F, N = 80 from two independent experiments. Scale bar = 2 μM. The
1210 statistical significance *p* value was estimated by the two-tailed student's t-test for the mean.

1211